Progenitors from the central nervous system drive neurogenesis in cancer

Philippe Mauffrey, Nicolas Tchitchek, Vilma Barroca, Alexis-Pierre Bemelmans, Virginie Firlej, Yves Allory, Paul-Henri Roméo, Claire Magnon

▶ **To cite this version:**

Philippe Mauffrey, Nicolas Tchitchek, Vilma Barroca, Alexis-Pierre Bemelmans, Virginie Firlej, et al.. Progenitors from the central nervous system drive neurogenesis in cancer. Nature, 2019, 569 (7758), pp.672-678. 10.1038/s41586-019-1219-y . cea-02186559

HAL Id: cea-02186559
https://cea.hal.science/cea-02186559v1

Submitted on 14 Nov 2022

HAL is a multi-disciplinary open access archive for the deposit and dissemination of scientific research documents, whether they are published or not. The documents may come from teaching and research institutions in France or abroad, or from public or private research centers.

L'archive ouverte pluridisciplinaire **HAL**, est destinée au dépôt et à la diffusion de documents scientifiques de niveau recherche, publiés ou non, émanant des établissements d'enseignement et de recherche français ou étrangers, des laboratoires publics ou privés.

ARTICLE

https://doi.org/10.1038/s41586-019-1219-y

Progenitors from the central nervous system drive neurogenesis in cancer

Philippe Mauffrey[1], Nicolas Tchitchek[2,7], Vilma Barroca[1,7], Alexis Bemelmans[3], Virginie Firlej[4], Yves Allory[4,5], Paul-Henri Roméo[6] & Claire Magnon[1]*

Autonomic nerve fibres in the tumour microenvironment regulate cancer initiation and dissemination, but how nerves emerge in tumours is currently unknown. Here we show that neural progenitors from the central nervous system that express doublecortin (DCX^+) infiltrate prostate tumours and metastases, in which they initiate neurogenesis. In mouse models of prostate cancer, oscillations of DCX^+ neural progenitors in the subventricular zone—a neurogenic area of the central nervous system—are associated with disruption of the blood–brain barrier, and with the egress of DCX^+ cells into the circulation. These cells then infiltrate and reside in the tumour, and can generate new adrenergic neurons. Selective genetic depletion of DCX^+ cells inhibits the early phases of tumour development in our mouse models of prostate cancer, whereas transplantation of DCX^+ neural progenitors promotes tumour growth and metastasis. In humans, the density of DCX^+ neural progenitors is strongly associated with the aggressiveness and recurrence of prostate adenocarcinoma. These results reveal a unique crosstalk between the central nervous system and prostate tumours, and indicate neural targets for the treatment of cancer.

Nerves are required during development, and for tissue repair and regeneration[1,2]. In the embryo, that development of the nervous system from the ectoderm is a pivotal event that acts in concert with developing haematopoietic and vascular systems to ensure homeostasis. The parallels between embryonic and tumour development suggests the existence of conserved regulatory pathways between normal and tumour microenvironments. As the development of the embryo requires neurogenesis, haematopoiesis and angiogenesis, so to do the initiation of primary tumours and onset of metastasis require the development of a nervous, immune and vascular network[1]. Neurogenesis involves the de novo production of functional neurons from neural precursors, and occurs—in rodents—throughout adult life in two neurogenic regions of the central nervous system; the subventricular zone (SVZ) that generates interneurons in the olfactory bulbs, and the dentate gyrus in the hippocampus, in which new dentate granule cells are generated[3]. Neurogenesis also occurs after brain injury and during tissue regeneration. Neural progenitors proliferate in the internal lumen of the central nervous system, the ventricular zone and the adjacent layer (that is, the SVZ), and the newborn neurons they generate migrate to injury sites to ensure a functional wound-healing response[4]. In tissue regeneration following the amputation of a salamander limb, innervation of the stump is necessary to fully rescue this amputation[2]. Newly formed nerve fibres infiltrate and expand in numerous solid cancers, including prostate, gastric, breast, pancreatic, colon and skin cancers[5–11]. Axonal outgrowth from pre-existing nerves is promoted by neurotrophic factors that are expressed and released within the tumour microenvironment, which builds up tumour-associated nerve networks that generate neural signalling for the regulation of tumorigenesis and metastasis[5,8,9,12]. In prostate cancer, the number of neurons per ganglia is increased, which suggests that a potential process of neurogenesis occurs in tumours and that this process supports tumour development and progression[13]. This process seems to be specific to cancer: in the healthy prostate, sympathetic innervation can regenerate after injury, which indicates a process of axonogenesis without any evidence for newly formed neurons[14]. In prostate cancer, the outgrowth of newly formed autonomic nerve fibres into the tumour contributes to the initiation and progression of cancer through the activation of β-adrenergic and muscarinic cholinergic signalling, respectively[5,8]. Surgical or chemical denervation of sympathetic adrenergic nerves inhibits the initiation of prostate tumours, and blockade of parasympathetic cholinergic nerve signalling decreases the spread of prostate cancer cells[5]. Similarly, denervation through vagotomy or ablation of cutaneous sensory nerves impairs the development of gastric cancer or non-melanoma forms of skin cancer, respectively[6,11]. Here we reveal a process of tumour-associated neo-neurogenesis in which neural progenitors leave the SVZ and reach—through the blood—the primary tumour or metastatic tissues, in which they can differentiate into new adrenergic neurons that are known to support the early stages of the development of cancer[5].

DCX^+ cells and tumour aggressiveness in human

DCX is a classical marker of neural progenitors that are located in developing and adult neurogenic regions of the central nervous system[15–17]. Stroma of human prostate primary tumours contained DCX^+ cells that also expressed specific markers of neural progenitors—polysialylated-neural cell adhesion molecule (PSA-NCAM)[18] and internexin[19,20] (Fig. 1a–e, Extended Data Fig. 1a)—but did not express markers of epithelial cells (pancytokeratin) (Fig. 1b) or mature nerve fibres (neurofilament-heavy[21]) (Fig. 1e, Extended Data Fig. 1a). To assess the potential clinical relevance of the neo-development of a neuronal network in prostate cancer, DCX^+ cells were quantified

[1]UMR967 (Laboratoire Cancer et Microenvironnement ATIP/AVENIR-INSERM-CEA), Institut de Radiobiologie Cellulaire et Moléculaire, Institut de Biologie François Jacob, Direction de la Recherche Fondamentale, Paris, France. [2]UMR1184 (INSERM-CEA-Université Paris Saclay), Infectious Diseases Models for Innovative Therapies, Institut de Biologie François Jacob, Direction de la Recherche Fondamentale, Paris, France. [3]UMR9199 (CNRS-CEA-Université Paris-Saclay), Molecular Imaging Research CENter, Institut de Biologie François Jacob, Direction de la Recherche Fondamentale, Paris, France. [4]Department of Pathology, Hôpital Henri-Mondor-Université Paris-Est, Paris, France. [5]Department of Pathology, Institut Curie, Paris, France. [6]UMR967 (INSERM-CEA-Université Paris Diderot-Université Paris Saclay), Laboratoire Réparation et Transcription dans les Cellules Souches, Institut de Radiobiologie Cellulaire et Moléculaire, Institut de Biologie François Jacob, Direction de la Recherche Fondamentale, Paris, France. [7]These authors contributed equally: Nicolas Tchitchek, Vilma Barroca. *e-mail: claire.magnon@cea.fr

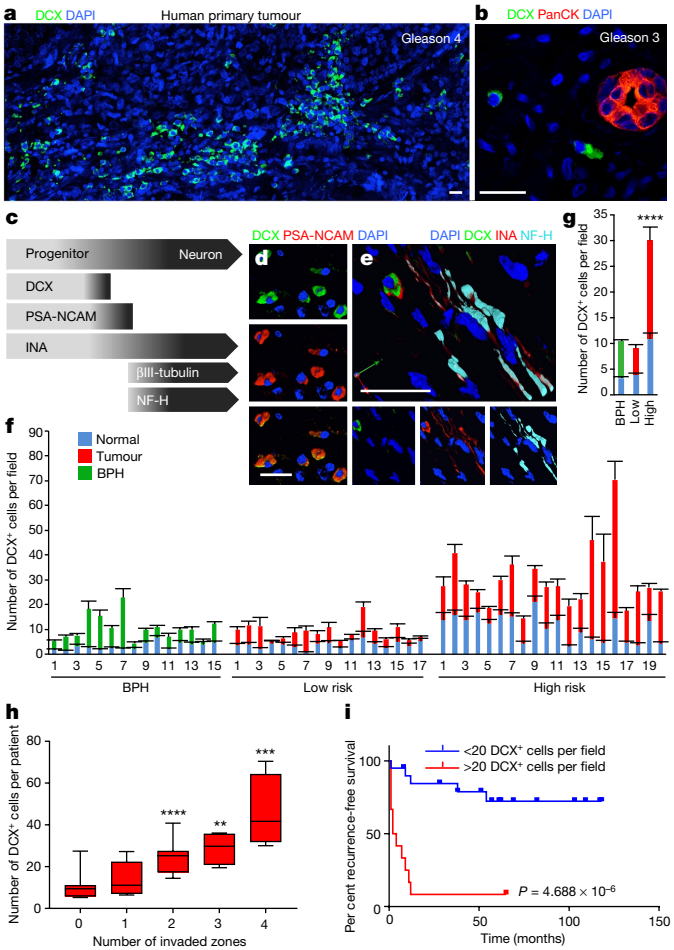

Fig. 1 | Prognostic value of stromal DCX$^+$ cells that infiltrate human prostate adenocarcinomas. a, **b**, DCX$^+$ cells in a Gleason grade 4 tumour area (**a**) and tumour epithelial pancytokeratin (panCK)-positive cells in a Gleason grade 3 tumour area (**b**). DCX, green; PanCK, red; DAPI, blue. Two independent experiments. Scale bars, 20 μm. **c**, Markers of neural progenitor differentiation into neurons. INA, internexin; NF-H, neurofilament-H. **d**, **e**, Confocal images showing that DCX$^+$ cells express early neural markers (PSA-NCAM (**d**, red) and INA (**e**, red)) but not the cytoskeletal subunit of NF-H, a marker of mature nerve fibres (light blue) in the central nervous system. DCX, green; DAPI, dark blue. Two independent experiments. Scale bars, 20 μm. **f**, **g**, Quantification of DCX$^+$ cells in benign prostatic hyperplasia (BPH, $n = 15$), and low-risk ($n = 17$) and high-risk ($n = 20$) human prostate adenocarcinomas. **f**, For each patient, the bar represents the average number of DCX$^+$ cells obtained from 10 fields per area for normal (blue), cancer (red) or hyperplastic (green) tissue, from total number of images for all the patients of 1,040 *z*-stack confocal images and with a field surface of 0.15 mm^2. Error bars indicate s.e.m. **g**, Average number of DCX$^+$ cells per field in normal (blue) and cancer (red) tissues of low-risk (low) or high-risk (high) patients, and in BPH areas (green) of the patient data shown in **f**. Wilcoxon rank-sum test (two-sided, no adjustment). Error bars indicate s.e.m. **h**. Association between the number of DCX$^+$ cells and the number of prostate areas (none, one, two, three or four) that are invaded by tumour cells. Box plots represent the median, and the first quartile and the third quartile of the number of DCX$^+$ cells per patient. Wilcoxon rank-sum test (no regions invaded, $n = 13$ patients; 1 region, $n = 7$ patients; 2 regions, $n = 10$ patients; 3 regions, $n = 4$ patients; and 4 regions, $n = 4$ patients)/ two-sided, no adjustment. **i**. Recurrence-free survival of patients with high (>20 DCX$^+$ cells per field) and low (<20 DCX$^+$ cells per field) numbers of DCX$^+$ cells. Mantel–Cox test ($n = 20$ patients for <20 DCX$^+$ cells per field; $n = 12$ patients for >20 DCX$^+$ cells per field). $^{**}P < 0.01$, $^{***}P < 0.001$, $^{****}P < 0.0001$.

in benign prostate hyperplasia from a cohort of 15 patients as well as in specimens from patients with low- and high-risk prostate cancer (17 low-risk, and 20 high-risk, treatment-naive patients with prostate cancer; Supplementary Table 1). The density of DCX$^+$ cells was significantly associated with tumour aggressiveness (Fig. 1f, g, Supplementary Table 2), invasion (Spearman's rank correlation coefficient = 0.7797; $P = 7.97 \times 10^{-9}$) (Fig. 1h, Supplementary Tables 3, 4) and recurrence ($P = 4.688 \times 10^{-6}$, log-rank (Mantel–Cox)) (Fig. 1i, Extended Data Fig. 1b), which suggests that DCX$^+$ cells may have a role in controlling the development and progression of prostate tumours in humans.

DCX$^+$ progenitors initiate tumour neurogenesis

DCX$^+$ cells were also present in the stroma of prostate cancer tissues of the Hi-MYC mouse model; Hi-MYC mice express human MYC under the control of the rat probasin promoter, specifically in prostate epithelial cells[5] (Extended Data Fig. 1c, d). To track, isolate and characterize DCX$^+$ cells in tumours from Hi-MYC mice, we generated a triple-transgenic mouse model of prostate cancer, in which the human *DCX* promoter and enhancer drive tamoxifen-inducible Cre expression of enhanced yellow fluorescent protein (eYFP) (*DCX-cre^{ERT2};loxp-eYFP* Hi-MYC mice) (Extended Data Fig. 2a). The presence of *DCX*–eYFP$^+$ cells in neurogenic areas (that is, the SVZ, olfactory bulbs and dentate gyrus) of the brain showed the recombination efficiency[22] (Fig. 2a, b, left, middle, Extended Data Fig. 2b). In prostate tumours, *DCX*–eYFP$^+$ cells found in the stromal compartment (Fig. 2b, right) were further characterized with the antigenic profile Lin$^-$ (lineage negative, CD45, TER119, CD31, CD326 and CD49f) (hereafter, Lin$^-$eYFP$^+$ (refs. [18,23,24]) (Extended Data Fig. 2c, d). These cells did not derive from tumour cells (Extended Data Fig. 2e) but did express SCA-1; prostate stromal cells are defined as Lin$^-$SCA-1$^+$ (Extended Data Fig. 3). The Lin$^-$eYFP$^+$ cells were found in prostate tumours but not in healthy prostate tissues from littermates without the *MYC* transgene (Fig. 2c), and expressed specific neural markers (PSA-NCAM, CD24 and EGFR) that were similar to those expressed by Lin$^-$eYFP$^+$ neural progenitors isolated from the SVZ, olfactory bulbs and dentate gyrus in the central nervous system[25,26] (Extended Data Fig. 3). Purified Lin$^-$eYFP$^+$ cells from tumours did not express markers of stem cells such as SOX2, musashi 1 (MSI1) and musashi 2 (MSI2)[27,28], or markers of activated neural stem cells (GFAP$^+$GLAST$^+$CD133$^+$EGFR$^+$MASH1$^{+/-}$nestin$^{+/-}$CD24$^{-/low}$ (superscript +/− and −/low denote mixed populations of cells)), but, instead, expressed markers of neural progenitors (GFAP$^-$GLAST$^-$CD133$^{-/low}$EGFR$^{-/low}$MASH1$^{-/low}$nestin$^+$CD24$^+$)[25,26] (Fig. 2d, e). Transcriptomic analysis of Lin$^-$eYFP$^+$ cells purified from tumours did not show any similarities with gene expression profiling of immune or endothelial cells (Extended Data Fig. 4a, Supplementary Table 5) but showed neuron-differentiation (Fig. 2f, right) and neuron-projection (Fig. 2f, left) signatures that were significantly similar to those of Lin$^-$eYFP$^+$ cells that were isolated from the SVZ or olfactory bulbs. Therefore, Lin$^-$eYFP$^+$ progenitors isolated from prostate tumours could proliferate and differentiate into newly born neurons ex vivo (Fig. 3a, Extended Data Fig. 4b–d). To explore the neurogenic capacity of these Lin$^-$eYFP$^+$ progenitors in vivo, as well as the stages of the Lin$^-$eYFP$^+$ neural-progenitor cell lineage, we performed inducible tissue-specific genetic tracing in prostate tumours. The activation of genetic recombination by tamoxifen at the third week after birth resulted in the presence of Lin$^-$eYFP$^+$ progenitors in prostate tumours, but not in the healthy tissues surrounding the prostate at weeks 8, 12 and 16 (tumour areas in Hi-MYC mice begin to develop 12 weeks after birth) (Fig. 3b, c, Extended Data Fig. 5 a, b), and the emergence of eYFP$^+$INX$^+$ nerve fibres from eYFP$^+$ neuroblasts at 8 months after birth (Fig. 3c, d). The eYFP$^+$ fibres also expressed tyrosine hydroxylase, which suggests that adrenergic neo-neurons can arise and develop in situ in the tumour microenvironment from Lin$^-$eYFP$^+$ progenitors (Fig. 3e). To document the differentiation stage of Lin$^-$eYFP$^+$ progenitors, two stromal sub-populations of eYFP$^+$ progenitor cells were purified from tumours of four-month-old mice on the basis of differential expression of SCA-1 in Lin$^-$eYFP$^+$PSA-NCAM$^+$ cells (hereafter, SCA-1^{low}PSA-NCAM$^+$ and SCA-1^{high}PSA-NCAM$^+$; Fig. 3f). The SCA-1^{high}PSA-NCAM$^+$ population expressed nestin, EGFR and MASH1, which are markers of activated progenitors from the SVZ; this

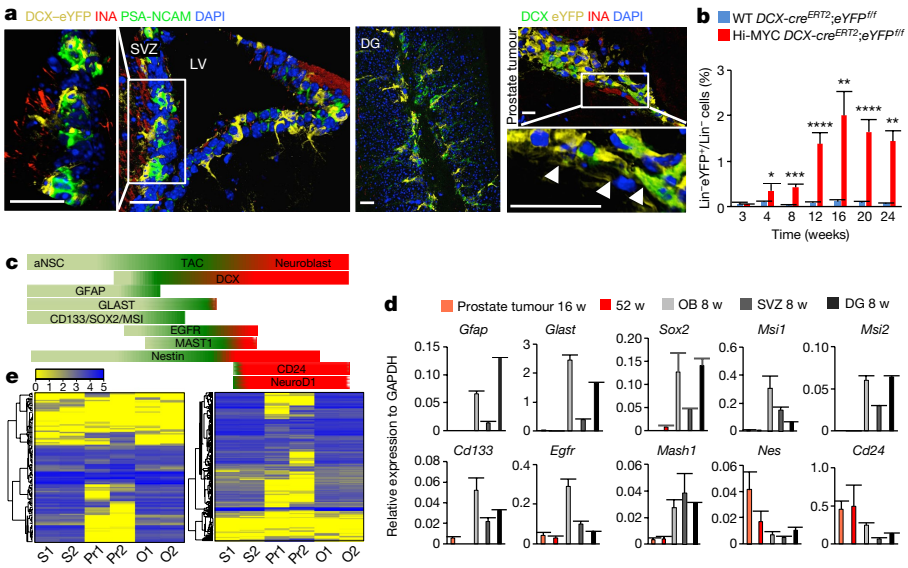

Fig. 2 | Hi-MYC prostate tumours contain *DCX*–eYFP$^+$ neural progenitors. a, Confocal images of *DCX*–eYFP$^+$ cells from *DCX-cre^{ERT2};loxp-eYFP* Hi-MYC mouse brain. Coronal sections of the SVZ (left) and dentate gyrus (DG) (middle) coexpressing PSA-NCAM (green) and INA (red), and from prostate cancer tissue (right) co-stained with anti-DCX (green) and anti-INA (red) antibodies. eYFP, yellow; DAPI, dark blue. eYFP$^+$ INA$^+$ nerve fibres branch off from *DCX*–eYFP$^+$ cells in tumours (white arrows). Three independent experiments. Scale bar, 20 μm. Regions in white boxes shown at higher magnification. LV, lateral ventricle. **b**. Frequency of Lin$^-$eYFP$^+$ cells among Lin$^-$ prostate stromal cells during cancer development. 3 weeks, $n = 8$ wild-type (WT) mice, $n = 11$ Hi-MYC mice; 4 weeks, $n = 9$ WT mice, $n = 28$ Hi-MYC mice; 8 weeks, $n = 9$ WT mice, $n = 26$ Hi-MYC mice; 12 weeks, $n = 14$ WT mice, $n = 11$ Hi-MYC mice; 16 weeks, $n = 8$ WT mice, $n = 12$ Hi-MYC mice; 20 weeks, $n = 9$ WT mice, $n = 14$ Hi-MYC mice; 24 weeks, $n = 9$ WT mice, $n = 20$ Hi-MYC mice. Data are mean + s.e.m. Student's *t*-test (one-sided, no adjustment). $^*P < 0.05$, $^{**}P < 0.01$, $^{***}P < 0.001$, $^{****}P < 0.0001$. **c**, Expression of neural markers in adult SVZ during (1) activation of neural stem cells (aNSC), (2) proliferation of transit-amplifying cells (TAC) and (3) generation of neuroblasts. **d**, Relative mRNA levels of neural markers shown in **c** in purified Lin$^-$eYFP$^+$ cells from prostate tumours, olfactory bulbs (OB), SVZ and dentate gyrus. Three independent experiments. Data are mean + s.e.m. Student's *t*-test (one-sided, no adjustment). W, weeks. *Glast* is also known as *Slc1a3*; *Mash1* is also known as *Ascl1*. **e**, Heat maps of genes involved in neuron differentiation (right) or neuron projection (left) in Lin$^-$eYFP$^+$ cells purified from the SVZ ($n = 2$ (S1, S2)), prostate tumour ($n = 2$ (Pr1, Pr2)) or olfactory bulbs ($n = 2$ (O1, O2)) of Hi-MYC mice. Spearman's test (two-sided, no adjustment), $P = 7.71 \times 10^{-7}$ and $P = 3.16 \times 10^{-20}$.

highlights a potential activated state for these SCA-1^{high}PSA-NCAM$^+$ progenitors[26] (such as transit-amplifying cells) (Fig. 3g). By contrast, the SCA-1^{low}PSA-NCAM$^+$ populations displayed a lower expression of neural progenitor markers but did express neuro-D1 (a transcription factor that is required for neuronal differentiation) and CD24, which suggests a neuroblast profile[26,29] (Fig. 3g). The frequencies of these two stromal populations fluctuated over time, which suggests that different stages of differentiation may occur during tumour development (Fig. 3h).

DCX$^+$ neural progenitors egress SVZ in tumorigenesis

During the development of prostate cancer in Hi-MYC mice, the number of Lin$^-$eYFP$^+$ neural progenitors in SVZ and olfactory bulb areas—but not in the dentate gyrus—oscillated significantly over time (Extended Data Fig. 5c, d). These oscillations were not associated with any change in the cellularity of the neurogenic areas of the brain, or with any increase of cell death—excluding the non-specific toxicity of tamoxifen (Extended Data Fig. 5e–g). Out of three subpopulations of Lin$^-$eYFP$^+$ neural progenitors (SCA-1$^-$PSA-NCAM$^-$, SCA-1$^{-/low}$PSA-NCAM$^+$ and SCA-1^{low}PSA-NCAM^{int}) in the SVZ area, only the SCA-1$^-$PSA-NCAM$^-$ population significantly oscillated during the development of cancer (Fig. 4a–b), and reached low levels at weeks 4, 12 and 20 after birth, by which point a population that expressed the same markers was present in large numbers in the tumour (SCA-1$^-$PSA-NCAM$^-$, green population in the prostate in Fig. 3f, h). Lineage tracing experiments confirmed oscillations of Lin$^-$eYFP$^+$ progenitors in the SVZ at 6 weeks after birth, and highlighted the presence of Lin$^-$eYFP$^+$ cells in the blood of 6-, 12- and 16-week-old Hi-MYC cancer-model mice (Extended Data Fig. 6a–d). These results suggested a potential egress of Lin$^-$eYFP$^+$SCA-1$^-$PSA-NCAM$^-$ neural stem and progenitor cells from the SVZ, which might give rise to Lin$^-$eYFP$^+$SCA-1$^-$PSA-NCAM$^-$ neural progenitors in the tumour. Of note, most of the Lin$^-$eYFP$^+$ populations in the SVZ expressed GFAP$^+$GLAST$^+$ stem and progenitor cell markers, whereas SCA-1$^-$PSA-NCAM$^-$ cells in tumours did not express these markers (Extended Data Fig. 6e). To provide evidence of this egress, stereotaxic injections of a tdTomato-expressing (tdTomato+) lentiviral vector into the SVZ of *DCX-cre^{ERT2};loxp-eYFP* Hi-MYC mice were performed to track progenitor cells that could emigrate from the SVZ towards the prostate tumour (Fig. 4c, d; Extended Data Fig. 7a–c). Lin$^-$tdTomato$^+$ cells were detected in the blood at the neoplastic stage of 6 weeks, and peaked in mice at the 8- and 16-week tumour stages (Fig. 4e); this provides support for the possible release of this population from the SVZ into the circulation. Subsequently, Lin$^-$tdTomato$^+$ cells were found in the tumours of 8-, 12- and 16-week-old mice but not in healthy tissues that surrounded the tumour, which shows that Lin$^-$tdTomato$^+$ cells selectively infiltrate prostate tumours (Fig. 4f, Extended Data Fig. 7d), in which they could differentiate into neurons (Fig. 4g, h). Associated with this egress, the blood–brain barrier adjacent to the lateral ventricle was breached in Hi-MYC mouse models of cancer but not in wild-type littermates, which suggests that—in these mouse models of cancer—neural progenitors may penetrate the blood–brain barrier through porous vasculature, and migrate away from the SVZ (Fig. 4i, Extended Data Fig. 7e). Injection of the tdTomato lentiviral vector into the dentate gyrus did not allow tdTomato$^+$ cells to reach the tumour, as they did when the lentiviral vector was injected into the SVZ (Extended Data Fig. 8a–c); this absence of egress from the dentate gyrus was associated with the lack of permeability of the vascularization of this region (Extended Data Fig. 8d, e).

We performed similar stereotaxic injections of a tdTomato-expressing lentiviral vector into the SVZ, using mouse models of PTEN[30] prostate cancer or PyMT[31] breast cancer; these models also displayed a

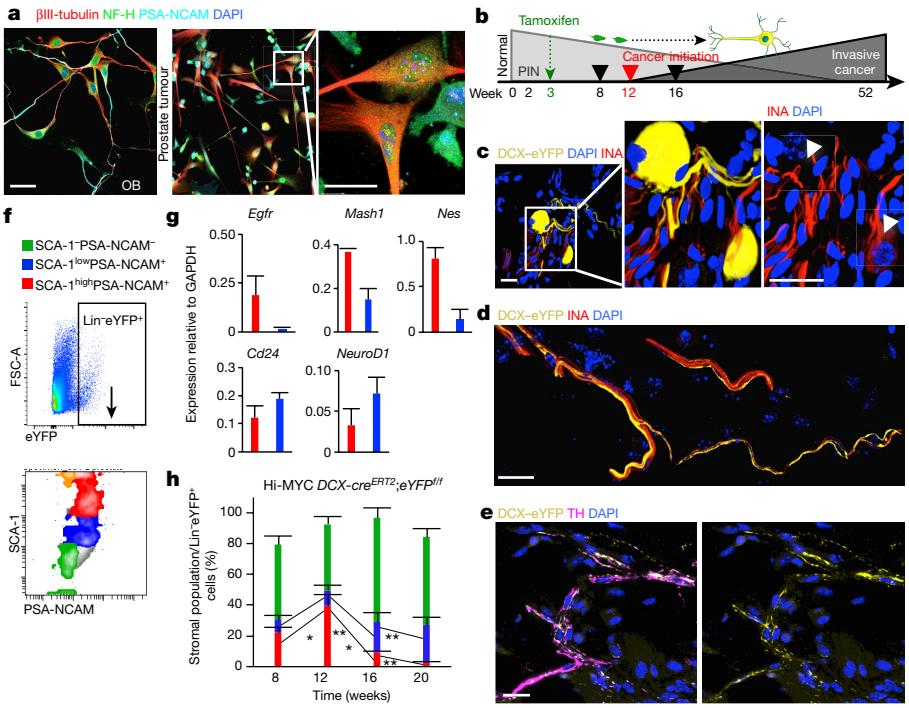

Fig. 3 | *DCX*–eYFP$^+$ neural progenitors can differentiate into adrenergic neurons in Hi-MYC prostate tumours. a, Ex vivo neuronal differentiation of *DCX*–eYFP$^+$ cells isolated from olfactory bulbs (OB) or prostate tumours (boxed area at higher magnification), and supplemented with epidermal growth factor and basic fibroblast growth factor. NF-H, green; PSA-NCAM, light blue; βIII-tubulin, red, DAPI, dark blue. Three independent experiments. Scale bars, 20 μm. **b**, Time course of tamoxifen injection in *DCX-cre^{ERT2};loxp-eYFP* Hi-MYC mice, and time of euthanasia. PIN, prostate intraepithelial neoplasia. **c**–**e**, *DCX*–eYFP$^+$ neural progenitors (yellow) in prostate tumour at five months after birth (boxed) area at higher magnification), *DCX*–eYFP$^+$ nerve fibres at eight months after birth co-stained with an anti-INA antibody (red) (**d**) and an anti-tyrosine hydroxylase antibody (TH, magenta) (**e**). DAPI, dark blue. Scale bars, 20 μm. **f**, Gating strategy of stromal SCA-1$^+$PSA-NCAM$^+$ cells (bottom) from Lin$^-$eYFP$^+$ prostate neural progenitors (top). **g**. Relative mRNA levels of neural differentiation markers in SCA-1^{low}PSA-NCAM$^+$ and SCA-1^{high}PSA-NCAM$^+$ populations defined in **f**. Data are mean + s.e.m. Student's *t*-test (one-sided, no adjustment). **h**, Temporal frequencies of the SCA-1$^+$ prostate stromal subpopulations in **f** at week 8 (prostate intraepithelial neoplasia), week 12 (cancer initiation) and week 16 and 20 (cancer development). Data are mean + s.e.m. Student's *t*-test (one-sided, no adjustment). 8 weeks, $n = 10$ mice; 12 weeks, $n = 8$ mice; 16 weeks, $n = 8$ mice; 20 weeks, $n = 4$ mice). $^*P < 0.05$, $^{**}P < 0.01$, $^{***}P < 0.001$, $^{****}P < 0.0001$.

significant accumulation of Lin$^-$tdTomato$^+$ cells in tumours, which indicates that the migration of neural progenitors is not restricted to tumours of Hi-MYC mice but might instead be a more general feature of the development of cancer (Extended Data Fig. 9a–c). Finally, we studied a range of metastatic tissues (colon, liver, lung and lymph nodes) in nude mice that were orthotopically xenografted with human luciferase-expressing PC3 (PC3-Luc) cancer cells. After stereotaxic injection of the tdTomato-expressing lentiviral vector into the SVZ, Lin$^-$tdTomato$^+$ cells were found only in the xenograft and metastatic tissues (the mean number of metastases were 18 per mouse (colon), five per mouse (liver and lymph nodes) and four per mouse (lung)) and not in healthy tissues (Extended Data Fig. 9d–g). This suggests a selective attraction and migration of neural progenitors in sites that are colonized by cancer cells, and this sustains the development of metastases.

DCX$^+$ neural progenitors regulate tumour development

To characterize the role of DCX$^+$ progenitors in the development of cancer, we crossed *DCX-cre^{ERT2}* mice with an inducible diphtheria toxin receptor (iDTR) line in a nude or Hi-MYC background to study the growth of luciferase-expressing, xenogeneic orthotopic (that is, PC3-Luc) tumours or Hi-MYC transgenic tumours, respectively. Selective depletion of DCX$^+$ cells after treatment with tamoxifen and diphtheria toxin significantly reduced the incidence of neoplastic lesions in Hi-MYC mice and inhibited the engraftment of PC3-Luc tumour cells, which suggests a critical role for DCX$^+$ cells in the early stages of tumour development (Fig. 5a–c, Extended Data Fig. 10). Further, selective depletion of progenitor cells in the SVZ by stereotaxic injection of diphtheria toxin within the SVZ induced a significant inhibition of tumour development (protocol 4 in Fig. 5a, Extended Data Fig. 10b). Conversely, orthotopic transplantation of purified Lin$^-$eYFP$^+$ cells—isolated from prostate tumours, the SVZ or olfactory bulbs—into established PC3-Luc xenografts resulted in increased tumour growth (Fig. 5d, e), the invasion of lymph nodes (Fig. 5f) and metastasis (Fig. 5g). To study the ability of the three subpopulations of neural progenitors and neuroblasts (SCA-1$^-$PSA-NCAM$^-$, SCA-1^{low}PSA-NCAM$^+$ and SCA-1^{high}PSA-NCAM$^+$ populations, isolated from prostate tumours, shown in Fig. 3f and described in Extended Data Fig. 7e) to promote tumour development and progression, we performed selective depletion experiments in *DCX-cre^{ERT2};iDTR* nude mice before grafting PC3-Luc cells together with each of the three purified subpopulations (Fig. 5h). As the transplantation of activated stem and progenitor cells induces faster kinetics of neuron formation than transplantation of quiescent cells[32], only the SCA-1^{high}PSA-NCAM$^+$ population promoted tumour growth seven weeks after transplantation (Figs. 3f, 5i); this provides support for interpreting them as exhibiting a activated progenitor-cell phenotype. Our results show major role of neural progenitors in prostate tumour development and indicate a population, the deletion of which might suppress the initial stages of development of both primary tumours and metastases.

Discussion

Numerous studies have established that cancer development depends on nerve fibre outgrowth[5–11], and that cancer cells may invade large nerves that surround the tumour to metastasize (a process called perineural invasion)[33]. These previous results clearly demonstrate dialogue between tumour development and nerves, but the origin of these nerves was not characterized. New neurons are continuously gen-

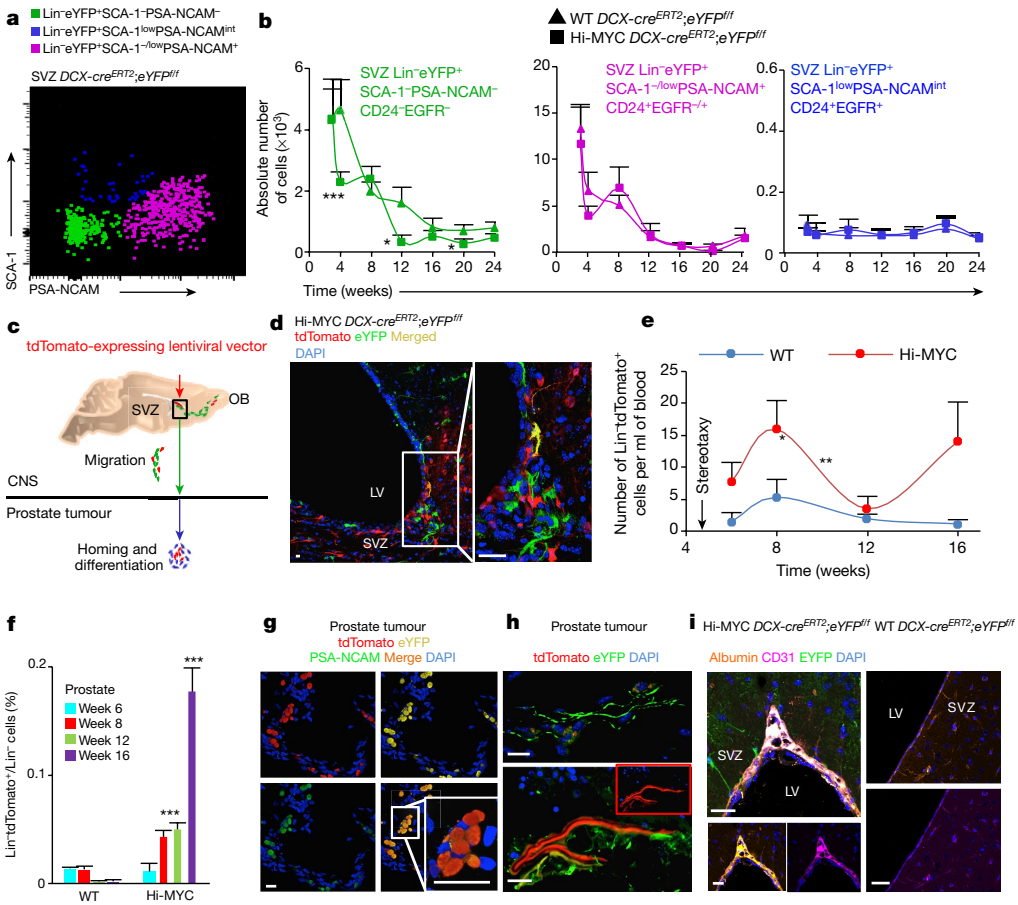

Fig. 4 | DCX$^+$ neural progenitors egress from the SVZ and migrate through the bloodstream towards prostate tumour in Hi-MYC mouse models of cancer. a, Fluorescence-activated cell sorting (FACS) plot of three subpopulations of neural progenitors purified from the SVZ of 8-week-old *DCX-cre^{ERT2};loxp-eYFP* transgenic Hi-MYC mice. **b**, Oscillations of Lin$^-$eYFP$^+$ progenitors in the SVZ of cancer mice (green, square) and wild-type littermates (green, triangle) at weeks 4, 12 and 20 after birth. Data are mean + s.e.m. Student's *t*-test (one-sided, no adjustment). 3 weeks, $n = 8$ WT mice, $n = 9$ Hi-MYC mice; 4 weeks, $n = 11$ WT mice, $n = 17$ Hi-MYC mice; 8 weeks, $n = 15$ WT mice, $n = 20$ Hi-MYC mice; 12 weeks, $n = 10$ WT mice, $n = 8$ Hi-MYC mice; 16 weeks, $n = 7$ WT mice, $n = 12$ Hi-MYC mice; 20 weeks, $n = 9$ WT mice, $n = 13$ Hi-MYC mice; 24 weeks, $n = 6$ WT mice, $n = 13$ Hi=MYC mice. **c**, Potential fate of brain neural progenitors after a stereotaxic injection of a tdTomato-expressing lentiviral vector into the SVZ (dotted box) of five-week-old *DCX-cre^{ERT2};loxp-eYFP* Hi-MYC mice. CNS, central nervous system. **d**, Coronal section of the SVZ (box at higher magnification) showing tamoxifen-induced eYFP$^+$ (green), lentiviral-vector-transduced tdTomato$^+$ (red, tdTomato$^+$) and eYFP$^+$tdTomato$^+$ (yellow) neural progenitors in the SVZ of five-month-old *DCX-cre^{ERT2};loxp-eYFP* Hi-MYC mice. Scale bar, 20 μm. **e**, **f**, After stereotaxic injection of the tdTomato$^+$ lentiviral vector into the SVZ at week five after birth, Lin$^-$tdTomato$^+$ cells circulate in the blood (**e**) and infiltrate prostate tumours (**f**). Data are mean s.e.m. Student's *t*-test (one-sided, no adjustment). Sample sizes are listed in Source Data. $^*P < 0.05$, $^{**}P < 0.01$, $^{***}P < 0.001$. **g**, **h**, Lin$^-$tdTomato$^+$ cells home in on the prostate tumour, in which tdTomato$^+$eYFP$^+$ cells express PSA-NCAM (green) (tdTomato, red; eYFP, yellow; DAPI, blue) (**g**), and differentiate into neurons in tumours six months later (tdTomato, red; eYFP, green; DAPI, blue) (**h**). **i**, Leaky vasculature (CD31, magenta) of the SVZ leads to the extravasation of albumin (orange) in brain tissues of one-year-old Hi-MYC cancer mice (left) but not in healthy littermates (right, eYFP, green; DAPI, blue).

erated throughout life in most mammals. In adult humans, neurogenesis may be most active in the striatum instead of the hippocampus—for which the lifelong generation of neo-neurons remains a point of controversy[34–36]. Striatal neurogenesis seems to be supplied by DCX$^+$PSA-NCAM$^+$ neural progenitors that are derived from the SVZ, the adjacent neurogenic area of the striatum[37,38]. Under pathological conditions (such as strokes), proliferation and neuronal production increase in the human SVZ and regenerate striatal neurons, which indicates that the SVZ is active throughout life[39,40]. Our results show that the SVZ may be hijacked during the development of cancer to provide neural progenitors that initiate neurogenesis during tumour formation. Further studies are necessary to characterize the cellular and molecular events that control the egress of neural progenitor cells from neurogenic niches in rodents and humans.

The central nervous system has previously been shown to regulate the function of peripheral organs, including leptin-dependent bone formation through the modulation of the sympathetic nervous system[39,40] and gut function in healthy and pathological conditions through the regulation of the autonomic nervous system[41]. The central nervous system may regulate the development and progression of cancer. Under stress conditions, the central nervous system can activate the autonomic nervous system or the hypothalamic–pituitary–adrenal axis; this results to the secretion of diverse mediators (such as glucocorticoids and catecholamines) that favour tumour initiation and progression[42]. Here we uncover crosstalk between the central nervous system and prostate or breast tumours, and reveal the unique migration of central neural progenitors that can differentiate as adrenergic neo-neurons: these neo-neurons nurture primary tumour development and metastasis. Together with a previous study that showed that lung tumours could drive distant granulopoiesis in bone (leading to the egress and migration of a neutrophil population to foster the tumour)[43], our results also show how a tumour could communicate with a distant organ to recruit cells that are required for its growth and dissemination.

Although clinical oncology studies have clearly pointed out the long-term cognitive decline of patients with cancer who are treated with chemotherapies that damage neural progenitor cells in the brain, our

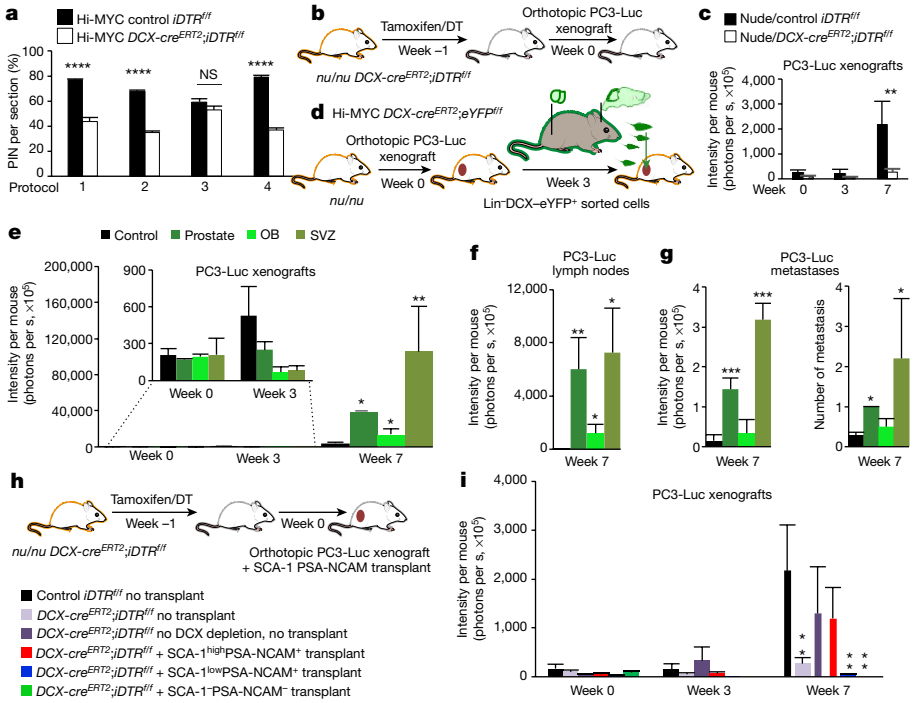

Fig. 5 | Initiation and progression of prostate cancer depend on DCX$^+$ neural progenitors. a, Effect of depletion of DCX$^+$ cells in *DCX-cre^{ERT2};iDTR* double- ('DCX mice') or control *iDTR* single-transgenic mice on incidence of prostate intraepithelial neoplasia at week 20 after birth, after tamoxifen and diphtheria-toxin treatments administered at early (intraperitoneal (IP) protocols 1, 2; SVZ protocol 4) or late (IP protocol 3) stages of tumour development. Percentages of prostate intraepithelial neoplasia were analysed from 10 sections per mouse. Protocol 1, $n = 7$ control mice, $n = 3$ DCX mice; protocol 2, $n = 14$ control mice, $n = 9$ DCX mice; protocol 3, $n = 5$ control mice, $n = 4$ DCX mice; protocol 4, $n = 8$ control mice, $n = 4$ DCX mice. Data are mean + s.e.m. Student's *t*-test (one-sided, no adjustment). **b**, **d**, **h**, Protocols used in **c**, **e**, **i**, respectively. **c**, PC3-Luc tumour growth measured by bioluminescence scanning with or without DCX$^+$ cells. Student's *t*-test (one-sided, no adjustment). $n = 8$ control mice, $n = 14$ DCX mice. **e**–**g**, Effect of transplantation of DCX$^+$ cells, purified from the prostate tumours, olfactory bulbs or SVZ on PC3-Luc tumour growth (**e**), invasion of lymph nodes (**f**) and growth and number of metastases (**g**). Data are mean + s.e.m. Student's *t*-test (one-sided, no adjustment). Sample sizes are listed in Source Data. **i**, After DCX$^+$ depletion, only transplantation of the Lin$^-$eYFP$^+$SCA-1^{high}PSA-NCAM$^+$ population purified from Hi-MYC prostate tumours rescued the growth of PC3-Luc tumours. Data are mean + s.e.m. Student *t*-test (one-sided, no adjustment). Sample sizes are listed in Source Data. $^*P < 0.05$, $^{**}P < 0.01$, $^{***}P < 0.001$, $^{****}P < 0.0001$.

study raises the possibility that the tumour itself might deplete neurogenic niches in the brain by attracting neural progenitors to support its own development, and suggests that treatment-naive patients with cancer may also develop cognitive impairment[44,45].

Taken together, these results open avenues for diagnosing and monitoring the development of cancer and suggest the potential of therapies that target neural progenitors in the tumour microenvironment.

Online content

Any methods, additional references, Nature Research reporting summaries, source data, statements of data availability and associated accession codes are available at https://doi.org/10.1038/s41586-019-1219-y.

Received: 15 February 2018; Accepted: 23 April 2019;
Published online 15 May 2019.

1. Eichmann, A. & Thomas, J. L. Molecular parallels between neural and vascular development. *Cold Spring Harb. Perspect. Med.* **3**, a006551 (2013).
2. Kumar, A. & Brockes, J. P. Nerve dependence in tissue, organ, and appendage regeneration. *Trends Neurosci.* **35**, 691–699 (2012).
3. Ming, G. L. & Song, H. Adult neurogenesis in the mammalian brain: significant answers and significant questions. *Neuron* **70**, 687–702 (2011).
4. Tanaka, E. M. & Ferretti, P. Considering the evolution of regeneration in the central nervous system. *Nat. Rev. Neurosci.* **10**, 713–723 (2009).
5. Magnon, C. et al. Autonomic nerve development contributes to prostate cancer progression. *Science* **341**, 1236361 (2013).
6. Zhao, C. M. et al. Denervation suppresses gastric tumorigenesis. *Sci. Transl. Med.* **6**, 250ra115 (2014).
7. Pundavela, J. et al. Nerve fibers infiltrate the tumor microenvironment and are associated with nerve growth factor production and lymph node invasion in breast cancer. *Mol. Oncol.* **9**, 1626–1635 (2015).
8. Dobrenis, K., Gauthier, L. R., Barroca, V. & Magnon, C. Granulocyte colony-stimulating factor off-target effect on nerve outgrowth promotes prostate cancer development. *Int. J. Cancer* **136**, 982–988 (2015).
9. Hayakawa, Y. et al. Nerve growth factor promotes gastric tumorigenesis through aberrant cholinergic signaling. *Cancer Cell* **31**, 21–34 (2017).
10. Stopczynski, R. E. et al. Neuroplastic changes occur early in the development of pancreatic ductal adenocarcinoma. *Cancer Res.* **74**, 1718–1727 (2014).
11. Peterson, S. C. et al. Basal cell carcinoma preferentially arises from stem cells within hair follicle and mechanosensory niches. *Cell Stem Cell* **16**, 400–412 (2015).
12. Cohen, S., Levi-Montalcini, R. & Hamburger, V. A nerve growth-stimulating factor isolated from sarcomas 37 and 180. *Proc. Natl Acad. Sci. USA* **40**, 1014–1018 (1954).
13. Ayala, G. E. et al. Cancer-related axonogenesis and neurogenesis in prostate cancer. *Clin. Cancer Res.* **14**, 7593–7603 (2008).
14. Kobayashi, T., Kihara, K., Hyochi, N., Masuda, H. & Sato, K. Spontaneous regeneration of the seriously injured sympathetic pathway projecting to the prostate over a long period in the dog. *BJU Int.* **91**, 868–872 (2003).
15. Francis, F. et al. Doublecortin is a developmentally regulated, microtubule-associated protein expressed in migrating and differentiating neurons. *Neuron* **23**, 247–256 (1999).
16. Couillard-Despres, S. et al. Doublecortin expression levels in adult brain reflect neurogenesis. *Eur. J. Neurosci.* **21**, 1–14 (2005).
17. Brown, J. P. et al. Transient expression of doublecortin during adult neurogenesis. *J. Comp. Neurol.* **467**, 1–10 (2003).
18. Zhang, J. & Jiao, J. Molecular biomarkers for embryonic and adult neural stem cell and neurogenesis. *BioMed Res. Int.* **2015**, 727542 (2015).
19. Kaplan, M. P., Chin, S. S., Fliegner, K. H. & Liem, R. K. Alpha-internexin, a novel neuronal intermediate filament protein, precedes the low molecular weight neurofilament protein (NF-L) in the developing rat brain. *J. Neurosci.* **10**, 2735–2748 (1990).
20. Schult, D. et al. Expression pattern of neuronal intermediate filament α-internexin in anterior pituitary gland and related tumors. *Pituitary* **18**, 465–473 (2015).

21. Carden, M. J., Trojanowski, J. Q., Schlaepfer, W. W. & Lee, V. M. Two-stage expression of neurofilament polypeptides during rat neurogenesis with early establishment of adult phosphorylation patterns. *J. Neurosci.* **7**, 3489–3504 (1987).
22. Walker, T. L., Yasuda, T., Adams, D. J. & Bartlett, P. F. The doublecortin-expressing population in the developing and adult brain contains multipotential precursors in addition to neuronal-lineage cells. *J. Neurosci.* **27**, 3734–3742 (2007).
23. Lawson, D. A. et al. Basal epithelial stem cells are efficient targets for prostate cancer initiation. *Proc. Natl Acad. Sci. USA* **107**, 2610–2615 (2010).
24. Ni, J. et al. Epithelial cell adhesion molecule (EpCAM) is associated with prostate cancer metastasis and chemo/radioresistance via the PI3K/Akt/mTOR signaling pathway. *Int. J. Biochem. Cell Biol.* **45**, 2736–2748 (2013).
25. Pastrana, E., Cheng, L. C. & Doetsch, F. Simultaneous prospective purification of adult subventricular zone neural stem cells and their progeny. *Proc. Natl Acad. Sci. USA* **106**, 6387–6392 (2009).
26. Chaker, Z., Codega, P. & Doetsch, F. A mosaic world: puzzles revealed by adult neural stem cell heterogeneity. *Wiley Interdiscip. Rev. Dev. Biol.* **5**, 640–658 (2016).
27. Suh, H. et al. In vivo fate analysis reveals the multipotent and self-renewal capacities of *Sox2*$^{+}$ neural stem cells in the adult hippocampus. *Cell Stem Cell* **1**, 515–528 (2007).
28. Sakakibara, S. et al. Mouse-Musashi-1, a neural RNA-binding protein highly enriched in the mammalian CNS stem cell. *Dev. Biol.* **176**, 230–242 (1996).
29. Boutin, C. et al. NeuroD1 induces terminal neuronal differentiation in olfactory neurogenesis. *Proc. Natl Acad. Sci. USA* **107**, 1201–1206 (2010).
30. Wang, S. et al. Prostate-specific deletion of the murine Pten tumor suppressor gene leads to metastatic prostate cancer. *Cancer Cell* **4**, 209–221 (2003).
31. Guy, C. T., Cardiff, R. D. & Muller, W. J. Induction of mammary tumors by expression of polyomavirus middle T oncogene: a transgenic mouse model for metastatic disease. *Mol. Cell. Biol.* **12**, 954–961 (1992).
32. Codega, P. et al. Prospective identification and purification of quiescent adult neural stem cells from their in vivo niche. *Neuron* **82**, 545–559 (2014).
33. Liebig, C., Ayala, G., Wilks, J. A., Berger, D. H. & Albo, D. Perineural invasion in cancer: a review of the literature. *Cancer* **115**, 3379–3391 (2009).
34. Sorrells, S. F. et al. Human hippocampal neurogenesis drops sharply in children to undetectable levels in adults. *Nature* **555**, 377–381 (2018).
35. Boldrini, M. et al. Human hippocampal neurogenesis persists throughout aging. *Cell Stem Cell* **22**, 589–599.e585 (2018).
36. Kempermann, G. et al. Human adult neurogenesis: evidence and remaining questions. *Cell Stem Cell* **23**, 25–30 (2018).
37. Ernst, A. & Frisén, J. Adult neurogenesis in humans–common and unique traits in mammals. *PLoS Biol.* **13**, e1002045 (2015).
38. Ernst, A. et al. Neurogenesis in the striatum of the adult human brain. *Cell* **156**, 1072–1083 (2014).
39. Ducy, P. et al. Leptin inhibits bone formation through a hypothalamic relay: a central control of bone mass. *Cell* **100**, 197–207 (2000).
40. Takeda, S. et al. Leptin regulates bone formation via the sympathetic nervous system. *Cell* **111**, 305–317 (2002).
41. Rhee, S. H., Pothoulakis, C. & Mayer, E. A. Principles and clinical implications of the brain–gut–enteric microbiota axis. *Nat. Rev. Gastroenterol. Hepatol.* **6**, 306–314 (2009).
42. Magnon, C. Role of the autonomic nervous system in tumorigenesis and metastasis. *Mol. Cell. Oncol.* **2**, e975643 (2015).
43. Engblom, C. et al. Osteoblasts remotely supply lung tumors with cancer-promoting SiglecF^{high} neutrophils. *Science* **358**, eaal5081 (2017).
44. Schagen, S. B. et al. Monitoring and optimising cognitive function in cancer patients: present knowledge and future directions. *EJC Suppl.* **12**, 29–40 (2014).
45. Dietrich, J. & Kesari, S. Effect of cancer treatment on neural stem and progenitor cells. *Cancer Treat. Res.* **150**, 81–95 (2009).

Acknowledgements We thank the iRCM animal facility and the MIRcen core facility for stereotaxy; J. Baijer for assistance with cell sorting and analysis; A Bourdais for technical assistance with preliminary data; and P. Soyeux for human tissue sectioning. This work was supported by a CEA/DRF/IBFJ/iRCM starting grant, the ATIP-AVENIR group leader program (INSERM, Ligue Contre le Cancer and Plan Cancer) and ARC.

Author contributions P.M. and V.B. performed experiments, N.T. analysed the RNA sequencing, and performed statistical analysis, A.B. produced lentiviral vectors and performed stereotaxic surgery, V.F. and Y.A. provided the cohort of patients, P.-H.R. wrote the manuscript, and C.M. designed, performed and supervised all the experiments, prepared figures and wrote the manuscript.

Competing interests A patent application, entitled 'Methods for predicting outcome and treatment of patients suffering from prostate and breast cancer', has been filed under the number EP18305460.0 on 13 April 2018, at the European Patent Office.

Additional information
Extended data is available for this paper at https://doi.org/10.1038/s41586-019-1219-y.
Supplementary information is available for this paper at https://doi.org/10.1038/s41586-019-1219-y.
Reprints and permissions information is available at http://www.nature.com/reprints.
Correspondence and requests for materials should be addressed to C.M.
Publisher's note: Springer Nature remains neutral with regard to jurisdictional claims in published maps and institutional affiliations.

© The Author(s), under exclusive licence to Springer Nature Limited 2019

METHODS

The experiments were not randomized. Investigators were not blinded to allocation; investigators were blinded during outcome assessment.

Mouse strains. Balb/c *nu/nu* (B6.Cg-*Foxn1*^{nu}) and Myc mice (FVB-Tg(ARR2/Pbsn-MYC)7Key (that is, Hi-MYC mice[5]) were obtained from Charles River laboratories and the National Cancer Institute, respectively.

Hi-MYC mice were intercrossed with C57BL/6-*Gt(ROSA)26Sortm1(eYFP)Cos* or C57BL/6-*Gt(ROSA)26Sortm1(HBEGF)Awai*/J mice, which were previously crossed with Tg(*DCX-cre/ERT2*)1Mul mice to generate Cre^{ERT2}-inducible expression of the enhanced yellow fluorescent protein (eYFP) or simian diphtheria toxin receptor (DTR) (from simian *Hbegf*) under the control of a DCX promoter (all obtained from the Jackson Laboratory). The resulting offspring, *DCX-cre*^{ERT2}*;loxp-eYFP* Hi-MYC or *DCX-cre*^{ERT2}*;loxp-HBEGF* Hi-MYC mice, express eYFP or DTR, respectively, in DCX-expressing cells after administration of tamoxifen to the mice. Cells expressing DTR can be ablated after diphtheria toxin administration. Respective controls were also generated by intercrossing the three strains.

Immunodeficient B6.Cg-*Foxn1*$^{nu+/-}$ heterozygous nude mice were also intercrossed with Tg(*DCX-cre/ERT2*)1Mul bred with *Gt(ROSA)26Sortm1(HBEGF)Awai*/J to deplete cells that express DCX in *nu/nu* mice.

Pten transgenic mice were generated by a specific *Pten* deletion (*Pten*$^{loxp/loxp}$) in prostate epithelial cells under the control of the probasin promoter (*ARR2Pbsn-cre, PB-cre4*)[30]. PyMT transgenic mice express the polyomavirus PyV middle T antigen specifically in mammary epithelial cells under the control of mouse mammary tumour virus (MMTV)[31].

Mouse procedures. All in vivo experiments were approved by the Animal Care and Use Committee of our institution (CEA/DRF/IBFJ/iRCM), authorized by the French Ministry of Research as referred to the authorization APAFIS#652-2015022617149597. Mouse housing, husbandry and care practices meet standards described in the animal welfare regulations and the guide for the care and use of laboratory animals (Directive EU 2010/63).

For *DCX-cre*^{ERT2}-mediated recombination, tamoxifen was prepared in corn oil (100 mg/kg, twice a day for 5 consecutive days) (Sigma-Aldrich) and was injected by intraperitoneal injection. For DCX^{+} cell-depletion experiments, diphtheria toxin (4 μg/kg, Sigma-Aldrich) was injected once daily intraperitoneally 48 h after the last tamoxifen injection, for 3 consecutive days.

For experiments in transgenic models, *DCX-cre*^{ERT2}*;loxp-EYFP* Hi-MYC mice were injected with tamoxifen at different time points between week 3 and week 24 after birth, and killed 2 weeks after the last injection of tamoxifen. For inducible genetic tracing experiments, *DCX-cre*^{ERT2}*;loxp-EYFP* Hi-MYC mice were injected at weeks 3 to 4 after birth, and mice were euthanized at 6, 8, 12 and 16 weeks after birth. For histological analyses after DCX^{+} cell depletion, *DCX-cre*^{ERT2}*;loxp-HBEGF* Hi-MYC animals were injected with tamoxifen (at week 3, week 4, week 8, week 12, week 16 after birth) and killed at week 20.

For the orthotopic xenogeneic model, human prostate tumours were induced by orthotopic surgical implantations of 1×10^5 PC3-Luc cells into 6-week-old Balb/c *nu/nu* mice. Three weeks after cell injection, the mice were randomized into groups and orthotopically received a vehicle or the appropriate transplant of purified Lin^{-}eYFP^{+} cells isolated from prostate tumour, olfactory bulbs or SVZ tissues. For DCX^{+} cell depletion experiments, 1×10^5 PC3-Luc cells were implanted orthotopically into tamoxifen-injected *DCX-cre*^{ERT2}*;loxp-HBEGF;nu/nu* mice (or control littermates), 2 days after the last injection of diphtheria toxin, with or without the co-transplantation of purified sub-populations of Lin^{-}eYFP^{+} cells isolated from prostate tumours of *DCX-cre*^{ERT2}*;loxp-EYFP* Hi-MYC mouse model of cancer.

Microdissection of the SVZ, olfactory bulbs and dentate gyrus from the adult mouse brain. After euthanasia, the heads of mice were cut off above the cervical spinal cord region, and a medial caudal–rostral cut was made to remove the skin of the head. The skull was peeled outward to expose the brain. The olfactory bulbs were first removed and collected in RPMI medium supplemented with 10% FBS (Life Technologies). Then, the brain was rotated to expose its ventral surface and the SVZ was isolated under a dissecting microscope, by first making a coronal cut at the level of the base of the optic chiasm and then making a second cut just before the hippocampus (Extended Data Fig. 2b), resulting to a coronal section from which the SVZ was collected and placed in RPMI medium supplemented with 10% FBS, as previously described.[46] The hippocampus containing the dentate gyrus was dissected from the remaining caudal part of the brain[47]. The medial surface of cerebral hemisphere was placed side-up to expose the medial side of the hippocampus. A needle tip was inserted at the boundary of the dentate gyrus and Ammon's horn, and slipped superficially along the septo-temporal axis of the hippocampus to isolate the dentate gyrus, which was collected in RPMI medium supplemented with 10% FBS.

Dissociation of brain and prostate tissues. Before being dissociated, prostate tissues were minced with a scalpel blade and then placed into a C tube for enzymatic dissociation. Brain and prostate tissues were enzymatically dissociated to single-cell suspensions into gentleMACS C tubes using the respective neural (T) or tumour tissue dissociation kits and the gentleMACS octo-dissociator with heaters. The gentleMACS programs NTDK_1 or m_TDK_1 were applied, respectively, as recommended by the manufacturer (Miltenyi Biotec). After dissociation, the cell suspension was applied to a MACS smartstrainer (70 μm), centrifuged and resuspended in MACS running buffer.

Cell culture. PC3 cells stably transfected with the luciferase 2 gene under the control of human ubiquitin C promoter (Catalogue number 128444/PC-3-luc2, Perkin Elmer), were grown in F12-glutamax medium supplemented with 10% FBS, 1.5 g/l bicarbonate sodium (Life Technologies). The authentication of PC3 cells was made by Perkin Elmer (source of parental line ATCC CRL-1435TM). All cell lines provided by Perkin Elmer are confirmed to be pathogen-free by the IMPACT profile I (PCR) at the University of Missouri Research Animal Diagnostic and Investigative Laboratory.

After enzymatic dissociation of olfactory bulbs and prostate cells from *DCX-cre*^{ERT2}*;loxp-eYFP* Hi-MYC mice, cells were washed, resuspended in MACS neuro medium (Miltenyi Biotec), and then 10^6 cells were plated into one well of a 24-well tissue culture plate (Thermo Fisher Scientific) that was previously coated with poly-L-ornithine (10 μg/ml, Sigma-Aldrich) and laminin (10 μg/ml, Corning Life Sciences). Half of the medium was replaced every 48 h for 1 week. Then, adherent cells were collected and passed onto poly-L-ornithine- and laminin-coated μ-slide 8 wells (Ibidi). Cells were incubated in MACS neuro medium supplemented with bFGF (20 ng/ml; Preprotech) and EGF (20 ng/ml; Preprotech) or brain-derived neurotrophic factor (BDNF, 1 μg/ml, Miltenyi Biotec) and neurotrophin-3 (NT-3, 0.1 μg/ml; Miltenyi Biotec). The medium was replaced every 48 h until neural differentiation of the cells.

Bioluminescence imaging. In vivo and ex vivo bioluminescence imaging was performed and analysed using an IVIS imaging system 200 series (Xenogen, Caliper Life Sciences). Bioluminescent signal was induced by intraperitoneal injection of D-luciferin (150 mg/kg in PBS) 7 min before in vivo imaging. For ex vivo imaging, D-luciferin (300 mg/kg) was injected 8 min before necropsy. Organs of interest were immersed in a solution of D-luciferin at 150 mg/ml. Disease development and progression were very closely monitored and metastatic mice were euthanized as soon as we noticed signs of discomfort in the mice, according to our approved IACUC protocol (bioluminescent signal does not exceed 10^{12} photons per s). In none of the experiments were these limits exceeded.

Histology and immunofluorescence. For paraffin-embedded sections, human and mouse prostate tissues were previously fixed in formalin or 4% paraformaldehyde, respectively. Blocks were serially sectioned (thickness of 5 μm) and haematoxylin and eosin (H&E) staining was performed using standard procedures. Before staining, sections were deparaffinized with xylene and rehydrated through graded alcohol washes followed by antigen retrieval in sodium citrate buffer following manufacturer recommendations (Vector Laboratories).

For frozen sections, mice were anaesthetized with 4% isoflurane before receiving a lethal dose of pentobarbital (60 mg/ml). Mice were then fixed by cardiac perfusion with 0.9% NaCl followed by 4% ice-cold paraformaldehyde (PFA) in 0.01 M PBS. The brain and prostate were collected, post-fixed overnight in 4% PFA at 4 °C and transferred in a 12% sucrose solution in PBS before snap-freezing and cryostat-sectioning (thickness of 12 μm; Leica).

For immunofluoresecnce, nonspecific binding was blocked with goat serum in BSA solution, and sections were incubated overnight with mouse antibodies to DCX (Millipore), to PSA-NCAM (ABC Scientific) or to pan-cytokeratin (Sigma-Aldrich), with rabbit antibodies to MAP-2 (Millipore), to βIII-tubulin (Covance), to α-internexin (Millipore), to tyrosine hydroxylase (Millipore) or to albumin (GeneTex), with rat antibody to CD31 (BioLegend) or with chicken antibodies to NF-H (Millipore) or to eYFP (Aves Laboratories). Secondary staining was subsequently performed for 1 h at room temperature with the appropriate Alexa Fluor 647-, 568- or 488-conjugated goat antibodies to mouse, rabbit, rat or chicken IgG, respectively (Life Technologies).

For dye administration, fluorescein-tagged albumin (65 kDa, 2 mg diluted in 0.1 ml saline; Sigma-Aldrich) and TRITC-tagged dextran (4.4 kDa, 2 mg diluted in 0.1 ml saline, Sigma-Aldrich) were simultaneously intravenously and intraperitoneally injected into five-month-old Hi-MYC mice under anaesthesia. After a circulation period of one hour, mice were deeply anaesthetized with isoflurane and pentobarbital, and euthanized by transcardial perfusion with 0.9% NaCl followed by 4% ice-cold PFA in 0.01 M PBS. Brains were collected, post-fixed overnight in 4% PFA at 4 °C and transferred in a 12% sucrose solution in PBS before snap-freezing and cryostat-sectioning (thickness of 14 μm; Leica).

Bright-field images of full Hi-MYC prostate sections were captured and collected with a Zeiss axioscan Z1 (Zeiss MicroImaging) equipped with an Hitachi HV-F202FCL colour camera controlled by Zen microscope software.

Fluorescence images were captured and analysed using a Leica TCS SP8 X confocal microscope equipped with white light laser, a PMT SP confocal detector coupled with a Leica hybrid detector for super-sensitive confocal imaging (Leica).

Images were obtained as 3D stacks scanning through the whole thickness of the tissue controlled by LAS X 2.0.1.14392 software and analysed using high-performance 3D imaging Volocity 6.3.1 software (Perkin Elmer).

Human prostate samples. Radical prostatectomies were obtained for staining after institutional review board approval at the Department of Pathology and Biological Resources Platform at Henri Mondor hospital (CPP no. 16169). Before signing the consent form, all patients were informed about the protocol and for the perspective of confidentiality, and all collected specimens were anonymized with an identification number before being released for clinical research. Human prostate tissues were collected, fixed in formalin and embedded in paraffin as part of routine care at Henri Mondor hospital (protocol no. DC2009-930). For each block, a section was stained with H&E to evaluate tissue viability, to localize normal areas among cancer and to map the different Gleason grade areas. All patients had histologically confirmed and clinically localized prostate cancer or benign hyperplasia, and did not received previous treatment at the institution. Patient characteristics, including age, preoperative prostatic specific antigen (PSA) levels, date of surgery, pathological stages and Gleason score, are shown in Supplementary Table 1. PSA recurrence was defined as a single PSA value at >0.2 ng/ml, 2 values at 0.2 ng/ml, or secondary treatment for a rising PSA. Recurrence might be local or distant, although no metastasis has been documented thus far in this cohort of patients. Extraprostatic extension was defined as disease involving one or more of extracapsular, ganglion, or seminal vesicle extension, and positive surgical margins. Quantification of DCX^+ cells was conducted blind (without knowledge of clinical data) in prostate tumour or hyperplastic areas, and in remaining normal prostate tissues surrounding areas of cancer. For each marker defined above, an average of 10 representative fields (one field = 0.15 mm^2) was calculated for normal areas, and for tumour grade captured as described above. A total of 1,040 *z*-stack images was acquired and converted in 2D maximum projections that were analysed with the Volocity software to quantify DCX^+/$DAPI^+$ cells per field (DAPI, 4′,6-diamidino-2-phenylindole).

Flow cytometry. The brain and prostate of *DCX-cre^{ERT2};loxp-eYFP* Hi-MYC mice were dissected and dissociated as described above. Cellularity of SVZ, olfactory bulbs, dentate gyrus and prostate were manually counted with viability in trypan blue using a Neubauer chamber before flow analysis.

Then, 10^6 cells were incubated for 10 min with FcR blocking reagent (Miltenyi Biotec). Subsequently, fluorochrome-conjugated monoclonal antibodies specific to mouse CD45 (clone 30F11), TER119 (clone Ter-119), CD31 (clone 390), CD326 (clone caa7-9G8), CD49f (clone REA518), SCA-1 (clone REA422), PSA-NCAM (clone 2-2B), CD24 (clone M1/69) were used for 20 min at the concentration recommended by the manufacturers (Miltenyi Biotec and BioLegend). Cells were also incubated with biotinylated EGF complexed with BV785-streptavidin (Invitrogen, Thermo Fisher Scientific). Analyses of stained cell suspensions were performed on a 5-laser SORP LSR II (355/408/488/561/640; BD BioSciences) and data were analysed with FlowJo software (Tree Star). The absolute number of cells was calculated as ((number of Lin^-eYFP^+ cells acquired × cellularity of the organ)/number of live single cells acquired).

RNA extraction, reverse transcriptase PCR and quantitative PCR. Gene expression levels were analysed from RNA extracted, using the RLT solution (Qiagen), from purified cells isolated from the 8-week-old brain or 16- and 52-week-old prostate of *DCX-cre^{ERT2};loxp-eYFP* Hi-MYC mice by quantitative real-time PCR. Reverse transcription (Superscript VILO; Invitrogen) was performed in accordance with the manufacturer's instructions. Quantitative PCR was performed with Fast SYBR Green (ABI Applied Biosystems, Thermo Fiscer scientific). Expression of glyceraldehyde-3-phosphate dehydrogenase (GAPDH) was used as a standard. Primer sequences are shown in Supplementary Table 6.

RNA sequencing. Lin^-eYFP^+ cells were isolated from 8-week-old brain or 16-week-old prostate of *DCX-cre^{ERT2};loxp-eYFP* Hi-MYC mice, and were collected in Qiazol (Qiagen). RNA was extracted using the miRNeasy microkit (Qiagen) and mRNA libraries were prepared using Smart-Seq v4 Ultra Low Input RNA (Takara). In brief, cDNA was synthesized by using the locked nucleic acid (LNA) technology integrated with SMART (switching mechanism at 5′ end of RNA template) technology. For each library, the cycle number after PCR with reverse transcription (RT–PCR) was adjusted according to the number of cells. Libraries were individually adapted and indexed using the Illumina Nextera XT kit and then were controlled on the Agilent Bioanalyzer (Tapestation 2200, Agilent Technologies). Identical libraries were pooled before sequencing at an average read depth of 70 million reads per sample. Final libraries were controlled on Tapestation 2200 (Agilent Technologies) and were quantified with fluorimetric intercalant. All RNA sequencing libraries were sequenced using the Illumina Nextseq 500 with HighOutPut cartridge to generate about 2 × 400 million of 75-base reads.

Sequenced reads were trimmed using trimmomatic version 0.36 based on a quality threshold of 33. Reads were aligned on the *Mus musculus* genome release GRCm38.p6 using ultrafast RNA-seq aligner STAR. Quantification of gene expression was performed using HTSeq version 0.10 based on default parameters and transcriptomic analyses were performed with the EdgeR package. The Gene Ontology (GO) term identifiers #GO:0043005 and #GO:0030182 were selected to study a list of genes associated with neuron projection and neuron differentiation. Hierarchical clustering in the heat map representations were generated based on the Ward 2 distance and the complete linkage method. Correlation analyses restricted to the selected lists of genes belonging to Gene Ontology were done using the Spearman coefficient of correlation, and the statistical significance was determined based on the associated *P* value. Expression analysis of genes in 53 Immunological Genome Project (ImmGen) populations listed in Supplementary Table 5 was performed using the ImmGen web portal (based on the MyGeneSet service, http://rstats.immgen.org/MyGeneSet_New/index.html). Statistical comparisons between SVZ, olfactory bulbs or prostate samples and ImmGen populations were performed based on the Spearman coefficient of correlation, restricted to the lists of 200 most highly expressed genes in each sample.

Stereotaxic injection. tdTomato cDNA was cloned under the control of the CAG promoter in a lentiviral shuttle plasmid that contains a self-inactivating HIV-1-derived genome. Recombinant lentiviral particles were produced by transient transfection of HEK-293T cells, and tittered by enzyme-linked immunosorbent assay (ELISA) quantification of the p24 capsid protein (HIV-1 p24 antigen ELISA). Before injection into the SVZ of 5-week-old Hi-MYC mice, viral particles were diluted in phosphate-buffered saline to a final concentration of 50 ng of p24 μl^{-1} and delivered in a volume of 2 µl by stereotaxic injection at the following coordinates: +0.7 mm anterior and +1.3 mm lateral relative to bregma; and −2.5 mm below the skull surface. Viral solution was injected at a speed of 0.2 $\mu l.min^{-1}$ and the injection cannula was left in place for 5 min before being slowly removed. The retroviral vector was injected in the dentate gyrus by stereotaxy at the following coordinates: 2 mm posterior and 1 mm lateral relative to bregma; and 2 mm below the skull surface.

Pten, PyMT and nude mice were injected by stereotaxy in the SVZ with the retroviral vector described above at the following coordinates: +1 mm anterior/posterior and ±1.3 mm lateral relative to bregma; and −2.5 mm ventral below the skull surface.

Statistical analyses. For mouse analyses, all values are reported as mean + s.e.m. Statistical significance was assessed by a parametric Student's *t*-test. Significance was set at $P < 0.05$. Statistical analyses were performed using GraphPad Prism (https://www.graphpad.com, v.7).

For patient studies, statistical analyses were performed using R software (https://www.r-project.org/, R Development Core Team, v.3.3). Statistical comparisons of the groups were performed using Wilcoxon rank-sum tests. The non-influence of patient ages on statistical comparisons was verified using regression analyses. Correlation between the number of DCX^+ cells and the number of invaded zones was identified using the Spearman coefficient of correlation. Survival curves were modelled using Kaplan–Meier estimates. The statistical significance of the difference between survival curves was then assessed using the log-rank (Mantel–Cox) test.

Data normality was evaluated using the Shapiro–Wilk test. All statistical tests used were two-sided. *P* values lower than 0.05 were considered as significant.

Reporting summary. Further information on research design is available in the Nature Research Reporting Summary linked to this paper.

Data availability

All data (Figs. 1–5, Extended Data Figs. 1, 2, 4–9) are available in the Article, Source Data or from the corresponding author on reasonable request. Raw fastq files are available on the EBI-ArrayExpress database, with the accession number E-MTAB-7727.

46. Guo, W., Patzlaff, N. E., Jobe, E. M. & Zhao, X. Isolation of multipotent neural stem or progenitor cells from both the dentate gyrus and subventricular zone of a single adult mouse. *Nat. Protoc.* **7**, https://doi.org/10.1038/nprot.2012.123 (2012).
47. Hagihara, H., Toyama, K., Yamasaki, N. & Miyakawa, T. Dissection of hippocampal dentate gyrus from adult mouse. *J. Vis. Exp.* **33**, e1543 (2009).

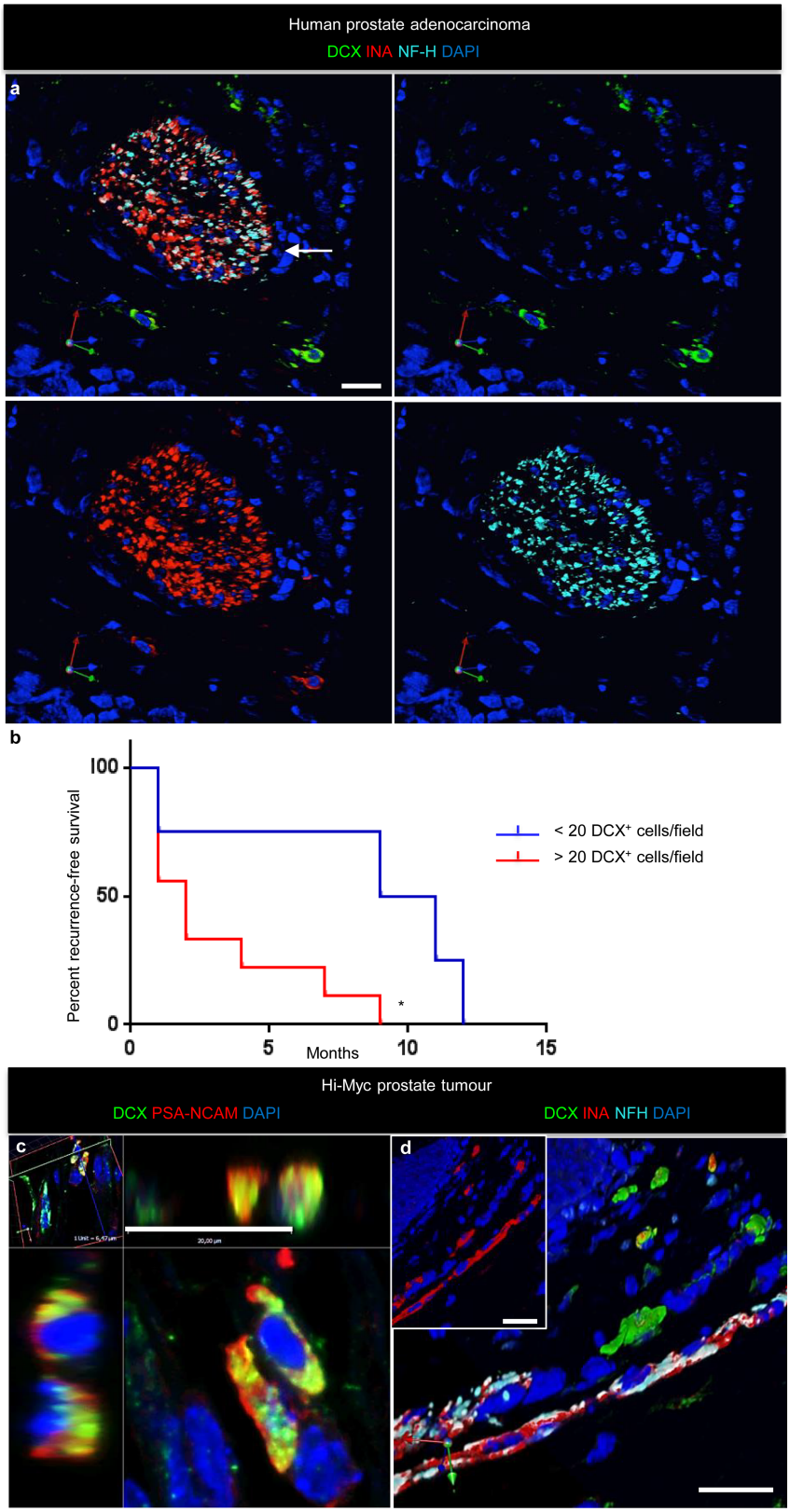

Extended Data Fig. 1 | DCX$^+$ cells express INA, a neural precursor marker, but not NF-H, a neuron-specific marker, in human prostate and Hi-MYC mouse prostate tumours, and are associated with tumour aggressiveness. a, In human adenocarcinoma, DCX$^+$ cells (green) and large peri-tumour nerve fibres (white arrow) express INA (red), a marker of developing neural cells and mature fibres. By contrast, mature nerve fibres express the neuron-specific cytoskeletal subunit of NF-H (light blue) but not DCX, a specific marker of neural progenitors in the central nervous system. DAPI, dark blue. Scale bar, 20 μm. **b**, Early time point analysis of recurrence-free survival of patients with high-risk prostate cancer. Early recurrence after radical prostatectomy is associated with high density of DCX$^+$ cells (>20 DCX$^+$ cells per field, $n = 13$). $P = 0.0338$, log-rank (Mantel–Cox). This is the same cohort of patients as shown in Fig. 1i, but here is focused on high-risk tumours. **c**, **d**, DCX$^+$ cells are also present in mouse prostate tumours and are stained for PSA-NCAM (red) (**c**) and INA (red) (**d**) but do not express mature nerve markers such as NF-H (light blue), which suggests that they are neural progenitors. DCX, green; DAPI, dark blue. Scale bar, 20 μm. Three independent experiments.

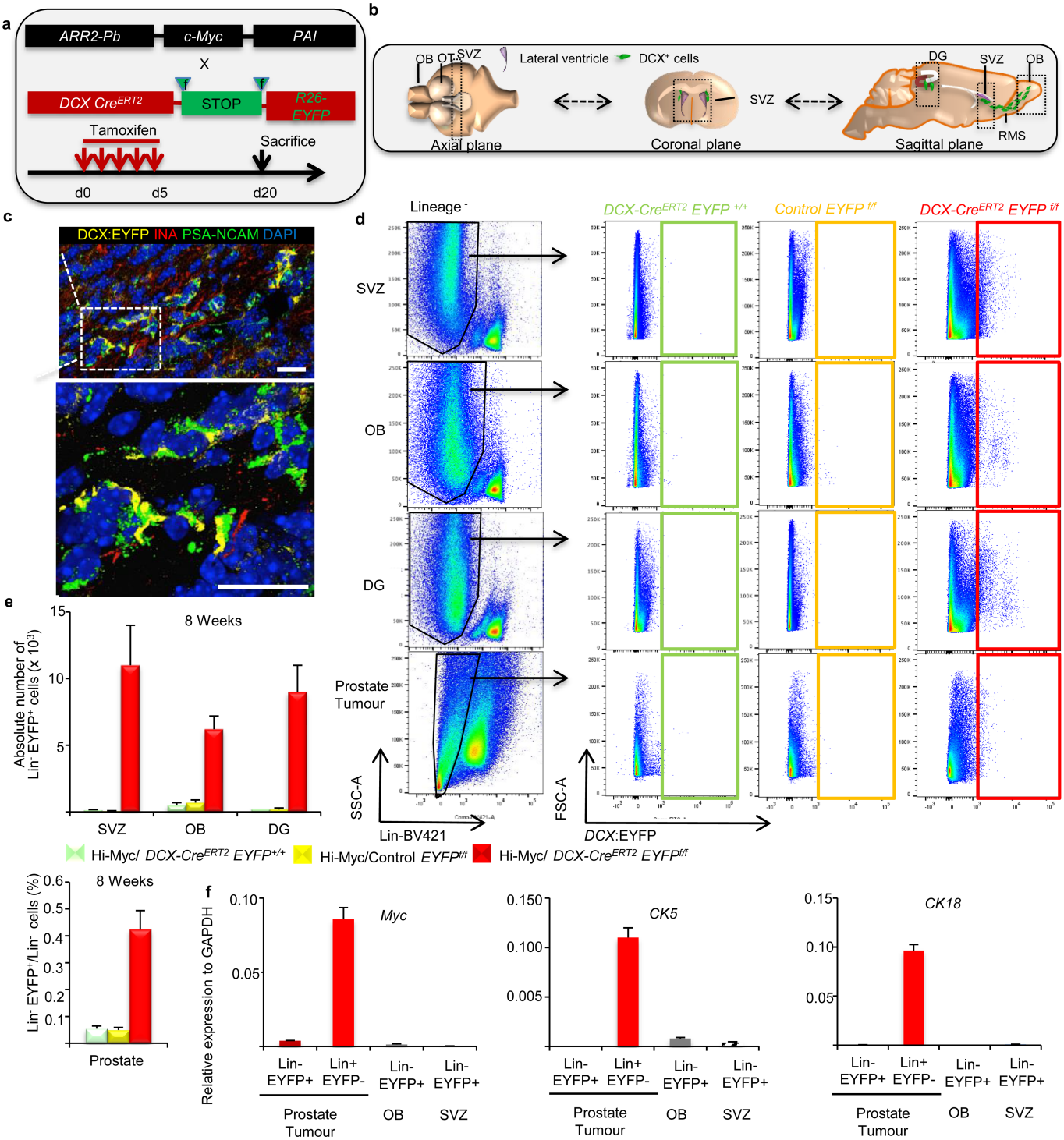

Extended Data Fig. 2 | Characterization and quantification of *DCX*–eYFP$^+$-expressing cells in a Cre-lox mouse model of cancer. **a**, Triple-transgenic *DCX-cre^{ERT2};loxp-eYFP* Hi-MYC mouse model of cancer mice is generated by crossing mice expressing MYC under the probasin promoter (AAR2/PBSN–MYC) with mice that express tamoxifen-inducible Cre^{ERT2} recombinase under the control of the DCX promoter/enhancer and bred with mice that have the *eYFP* gene inserted in the *Gt(Rosa)26Sor* locus with an upstream loxP-flanked STOP sequence (top). Timeline of tamoxifen injections (bottom). **b**. Schematics of axial, coronal and sagittal sections of the adult mouse brain showing the olfactory bulbs and olfactory tract (OT), the SVZ along the lateral ventricle, and the dentate gyrus. **c**. Images of *DCX*–eYFP$^+$ neural precursors (yellow), in olfactory bulbs, from mice described in **a**, co-stained with anti-PSA-NCAM (green) and anti-INA (red) antibodies. DAPI, dark blue. Scale bar, 20 μm. Three independent experiments. **d**, FACS plots of eYFP$^+$ cells isolated from Lin$^-$ cells from the brain (SVZ, olfactory bulbs, dentate gyrus and tumour tissues of *DCX-cre^{ERT2};loxp-eYFP* Hi-MYC mice (red) compared to control littermates (green and yellow). **e**, Quantification of Lin$^-$eYFP$^+$ cells in SVZ, olfactory bulbs and dentate gyrus (top) and prostate tumour (bottom). Data are mean + s.e.m. Student's *t*-test (one-sided, no adjustment). Sample sizes are listed in Source Data. **f**, Lin$^-$eYFP$^+$ cells in Hi-MYC prostate tumours do not derive from tumour cells. Real-time quantitative PCR analyses of mRNA extracted from Lin$^-$eYFP$^+$ cells isolated from prostate tumour tissues, olfactory bulbs and the SVZ of *DCX-cre^{ERT2};loxp-eYFP* Hi-MYC mice. The Lin$^-$eYFP$^+$ cells do not express *MYC* oncogene or the cytokeratins (CK5 and CK18) present in the Lin$^+$eYFP$^-$ fraction that comprises prostate epithelial cells. Data are mean + s.e.m.

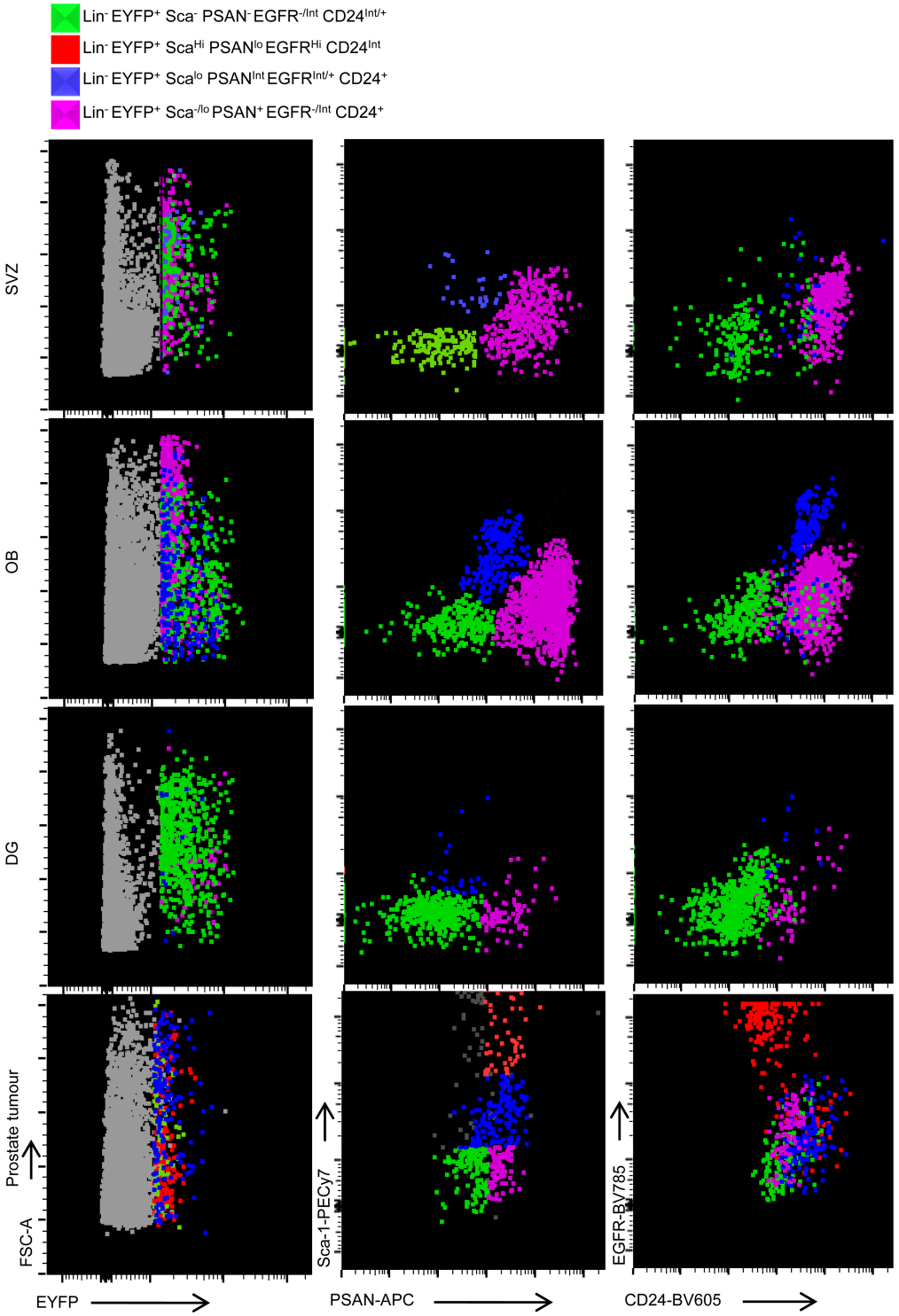

Extended Data Fig. 3 | Lin$^-$eYFP$^+$ cells in prostate tumours express markers of neural precursors from the central nervous system. Representative FACS plots of SCA-1, PSA-NCAM, CD24 and EGFR expression in neural Lin$^-$eYFP$^+$ subpopulations from the brain at week eight after birth (SVZ, olfactory bulbs and dentate gyrus) and the prostate tumour at four months after birth. Note that two subpopulations of Lin$^-$eYFP$^+$ cells from prostate tumours express SCA-1 (prostate stromal cells are Lin$^-$SCA-1$^+$). Representative data from 48 independent experiments.

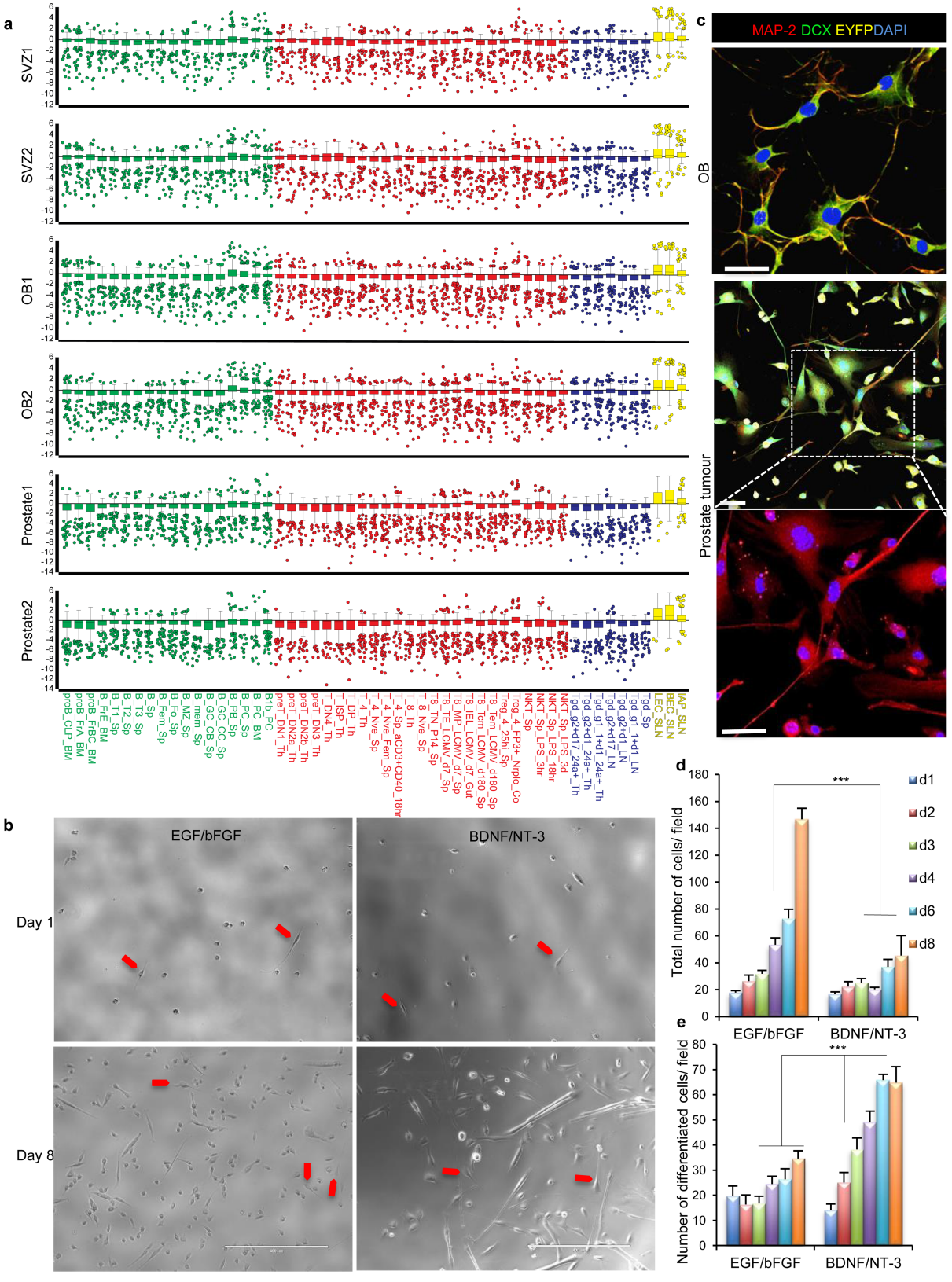

Extended Data Fig. 4 | See next page for caption.

Extended Data Fig. 4 | *DCX*–eYFP$^+$progenitors in prostate tumours can proliferate and/or differentiate into neurons ex vivo. a, Lin$^-$eYFP$^+$ cells do not display immune or endothelial phenotypes. Scatter plot representations (also known as ImmGen W-plots) of the mean-normalized expression values of the 200 most-highly expressed genes of each sample (SVZ, olfactory bulb or prostate, $n = 2$ per region) in each of the selected ImmGen cell populations. ImmGen populations are coloured on the basis of their main cell population families, listed in Supplementary Table 5 with correlation coefficients and *P* values. **b**, Differentiation of *DCX*–eYFP$^+$ cells from prostate tumour tissues after one or eight days culture in neural medium supplemented with epidermal growth factor and basic fibroblast growth factor (EGF and bFGF, proliferation medium), or brain-derived neurotrophic factor and neurotrophin-3 (BDNF and NT-3, differentiation medium). Scale bar, 400 μm. Two independent experiments. **c**, Immunostaining of MAP2$^+$ differentiated *DCX*–eYFP$^+$ neural cells isolated from tumour (right) or olfactory bulbs (left). Scale bar, 20 μm. Three independent experiments. **d**, **e**, Quantification of proliferation of neural progenitors (**d**) and differentiated neural cells (**e**) with one or more neurites (red arrows (for example in **b**)) for eight days. Data are mean + s.e.m. Student's *t*-test (one-sided, no adjustment). ***$P < 0.001$. Two independent experiments.

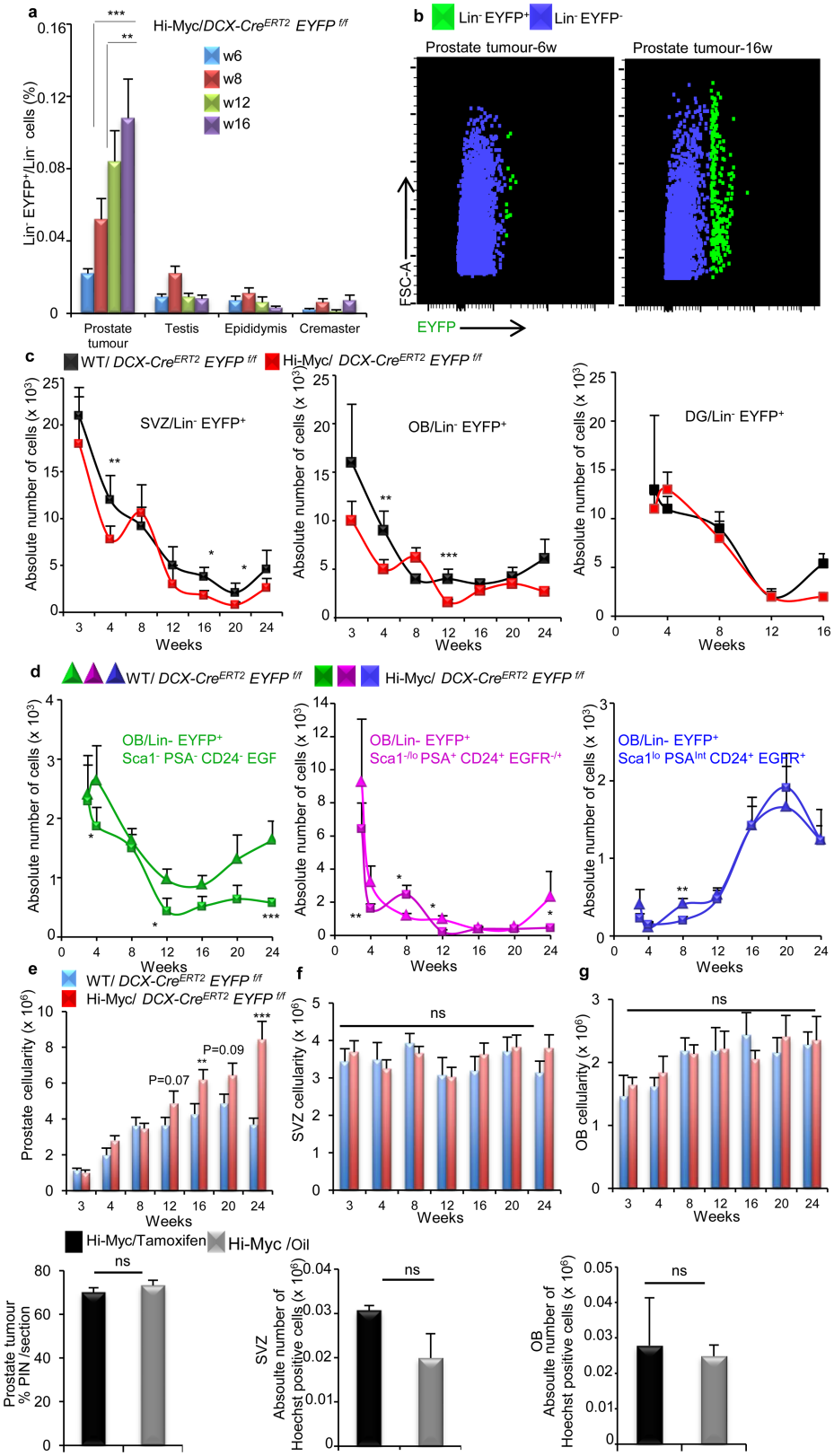

Extended Data Fig. 5 | See next page for caption.

Extended Data Fig. 5 | Genetic lineage tracing of Lin$^-$eYFP$^+$ progenitors during prostate development. a, After tamoxifen-induced recombination of *DCX-cre^{ERT2};loxp-eYFP* Hi-MYC cancer mice at week 3 after birth, Lin$^-$eYFP $^+$ neural progenitors are detected in tumour tissues during the early phases of cancer development, without infiltrating healthy tissues ($n = 73$), such as testis ($n = 34$), epididymis ($n = 35$) and cremaster ($n = 29$), that surround the tumour. Data are mean + s.e.m. Student's *t*-test (one-sided, no adjustment). Twelve independent experiments. Sample sizes per group are listed in Source Data. **b**, FACS plots of Lin$^-$eYFP$^+$ cells from the prostate tumour of 6- or 16-week-old Hi-MYC mice. **c**, Oscillation of Lin$^-$eYFP$^+$ neural progenitors during prostate tumour development in the SVZ (left, $n = 163$) and olfactory bulbs (middle, $n = 159$), but not in the dentate gyrus (right, $n = 59$) of Hi-MYC cancer mice. Data are mean + s.e.m. Student's *t*-test (one-sided, no adjustment). Forty-six independent experiments. Sample sizes per group are listed in Source Data. **d**, Further monitoring shows marked oscillations of Lin$^-$eYFP$^+$SCA-1$^-$PSA-NCAM$^-$CD24$^-$EGFR$^-$ cells present in the olfactory bulbs, as observed in SVZ in Fig. 4b. Data are mean + s.e.m. Student;s *t*-test (one-sided, no adjustment). Forty-six independent experiments. Sample sizes are listed in Source Data. **e**–**g**, Tamoxifen is not cytotoxic to prostate or brain tissues, as shown by the fact that it does not affect the development of tumours in the Hi-MYC mouse model of cancer (**e**) and does not alter the cellularity (top) and viability (bottom) of cells in SVZ (**f**) or olfactory bulbs (**g**) over time. Data are mean + s.e.m. Student's *t*-test (one-sided, no adjustment). Sample sizes are listed in Source Data. $^*P < 0.05$, $^{**}P < 0.01$, $^{***}P < 0.001$.

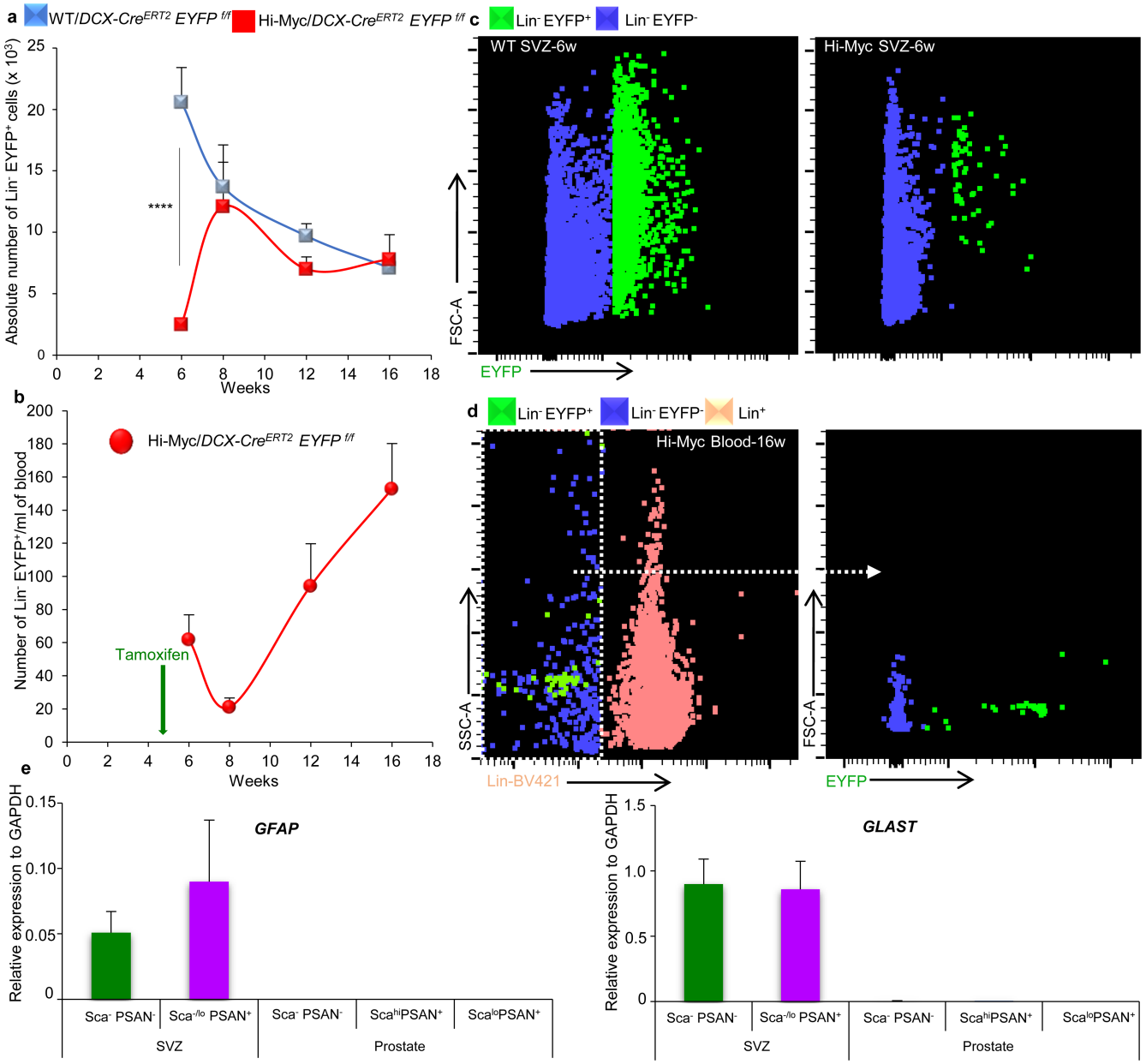

Extended Data Fig. 6 | In Hi-MYC mouse model of cancer, Lin$^-$eYFP$^+$ progenitors egress the SVZ, migrate through the blood and infiltrate the tumour, where they do not express neural stem-cell markers. **a**, **b**, After tamoxifen-induced recombination in the *DCX-cre^{ERT2};loxp-eYFP* Hi-MYC cancer mice at week 3 after birth, the number of Lin$^-$eYFP$^+$ neural progenitors decreases in the SVZ at week 6 after birth (**a**) and—in turn—Lin$^-$eYFP$^+$ cells emerge progressively in blood (**b**). Data are mean + s.e.m. Student's *t*-test (one-sided, no adjustment). Sample sizes are listed in Source Data. Thirteen independent experiments. **c**, **d**, Representative FACS plots of Lin$^-$eYFP$^+$ cells isolated from the SVZ (**c**) or blood (**d**) of 6- or 16-week-old wild-type or Hi-MYC mice. ****$P < 0.0001$. **e**, Lin$^-$eYFP$^+$SCA-1$^-$PSA$^-$NCAM$^-$ cells in the SVZ—but not in prostate tumours—express neural stem-cell markers. Real-time quantitative PCR analyses of mRNA extracts obtained from purified subpopulations of the SVZ and prostate tumour tissues of *DCX-cre^{ERT2};loxp-eYFP* Hi-MYC mice. The Lin$^-$eYFP$^+$SCA-1$^-$PSA$^-$NCAM$^-$ cells from the SVZ express GFAP and GLAST, which are specific markers of neural stem cells. By contrast, Lin$^-$eYFP$^+$SCA-1$^-$PSA$^-$NCAM$^-$ cells in tumours do not express the stem-cell markers. Three independent experiments. Data are mean + s.e.m.

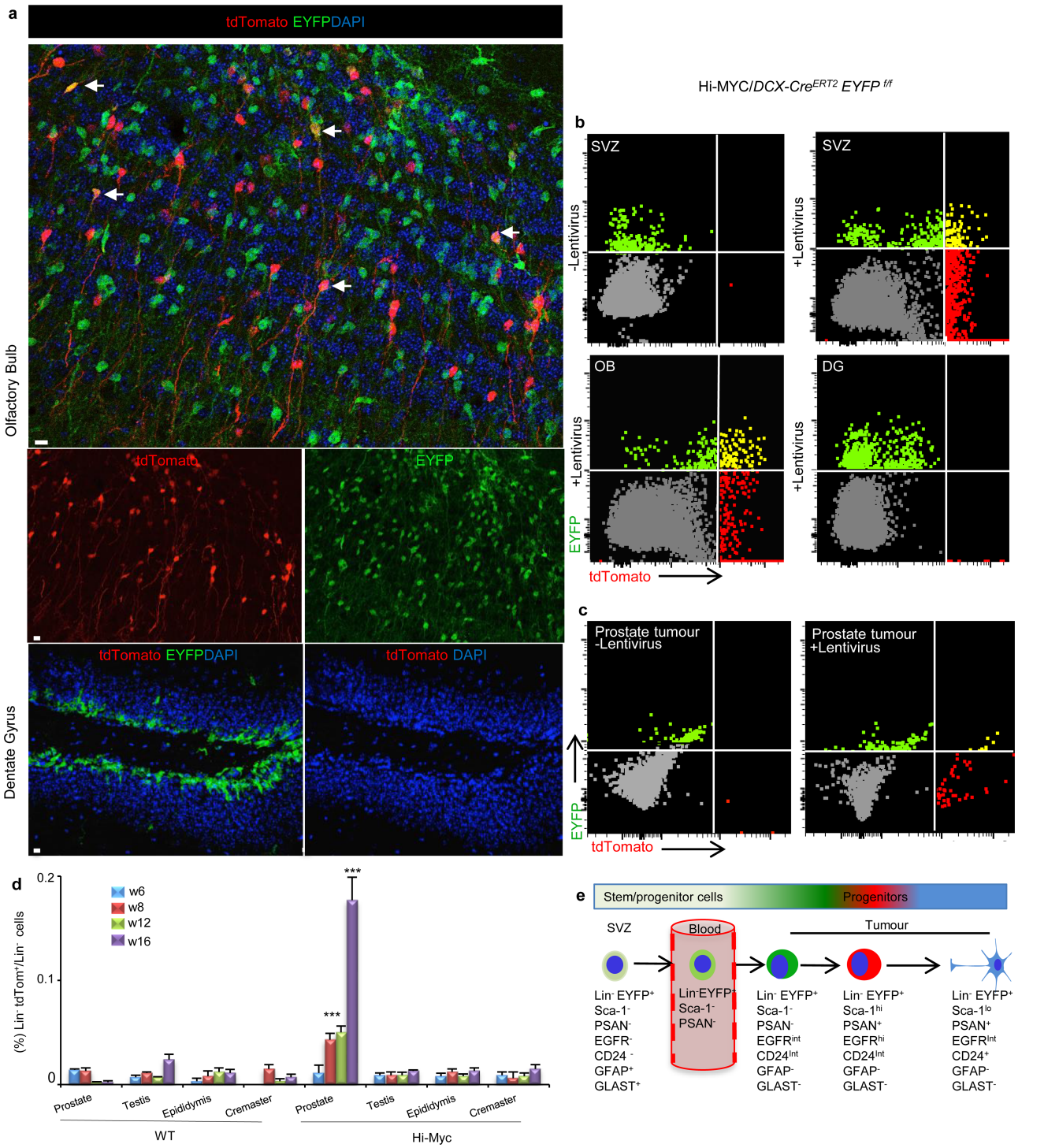

Extended Data Fig. 7 | tdTomato-expressing neural precursors migrate from the SVZ towards olfactory bulbs. a, Immunostaining of neural precursors, transduced by a tdTomato-expressing lentiviral vector administered by stereotaxic injection into the SVZ of tamoxifen-injected *DCX-cre^{ERT2};loxp-EYFP* Hi-MYC cancer mice, tdTomato^{+} cells leave the SVZ to reach the olfactory bulb area through the physiological rostral migratory stream, and differentiate into neurons in olfactory bulbs (top, white arrows, tdTomato^{+}eYFP^{+} cells). Note that these tdTomato-expressing neural cells do not spread in the dentate gyrus (bottom). Scale bars, 20 μm. **b**, **c**, FACS plots showing tamoxifen-induced eYFP^{+} (green), lentiviral vector-transduced tdTomato^{+} (red, tdTomato^{+}) and eYFP^{+}tdTomato^{+} (yellow) neural precursors in the SVZ, olfactory bulbs and dentate gyrus of five-month-old Hi-MYC mice (**b**) and infiltration of these cells into prostate tumours (**c**). **d**, Lineage tracing of Lin^{-}tdTomato^{+} cells that infiltrate prostate tumours but not healthy tissues surrounding the tumour (testis, epididymis and cremaster). Data are mean + s.e.m. Student's *t*-test (one-sided, no adjustment). Sample sizes are listed in Source Data. ***$P < 0.001$. **e**, Summary of the five developmental stages of neural progenitors migrating (through the blood) from the central nervous system to the tumour during cancer development. tdTom^{+}, tdTomato^{+}.

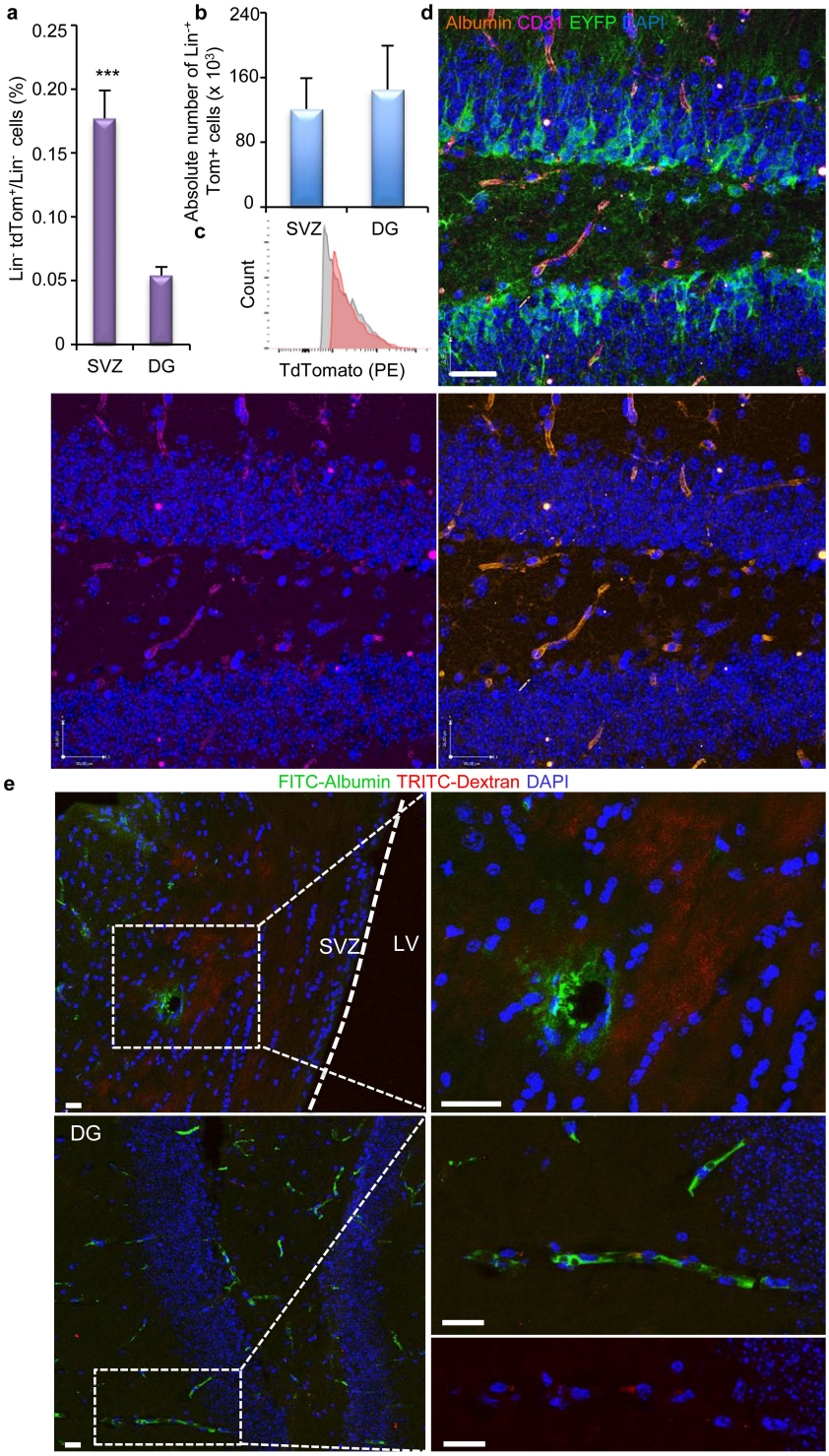

Extended Data Fig. 8 | Lin$^-$tdTomato$^+$ cells cannot reach the tumour after lentiviral injection in the dentate gyrus. a, Frequencies of Lin$^-$tdTomato$^+$ cells in prostate tumours at 16 weeks of age, after tdTomato$^+$ lentiviral vector injection by stereotaxy into the dentate gyrus ($n = 6$) at week 5 after birth, by comparison to an injection into the SVZ ($n = 10$ mice). Data are mean + s.e.m. Student's *t*-test (one-sided, no adjustment). ***$P < 0.001$. **b**, Absolute numbers of Lin$^-$tdTomato$^+$ cells in the SVZ ($n = 9$) or dentate gyrus ($n = 8$) 16 weeks after the injection of the tdTomato$^+$ lentiviral vector in the respective brain area. Data are mean + s.e.m. **c**. Respective mean fluorescence intensities (MFI) for tdTomato signal in SVZ (MFI/SVZ, red) and dentate gyrus (MFI/DG, grey) shown in **b**. **d**, Dentate gyrus vascularization (CD31$^+$, pink) in one-year-old Hi-MYC mice does not exhibit any leakiness of albumin (orange) in the dentate gyrus. *DCX*–eYFP$^+$ cells (green). DAPI, dark blue. Scale bar, 30 μm. **e**, The blood–brain barrier is breached in the SVZ of Hi-MYC cancer mice. Combined injection of fluorescein–albumin (65 kDa, green) and TRITC–dextran (4.4 kDa, red) reveals extravasation of both dyes in SVZ tissues (top) throughout sinusoids. In the dentate gyrus, the dyes do not spread outside of the capillaries (bottom). DAPI, dark blue. Scale bars, 20 μm. tdTom$^+$, tdTomato$^+$.

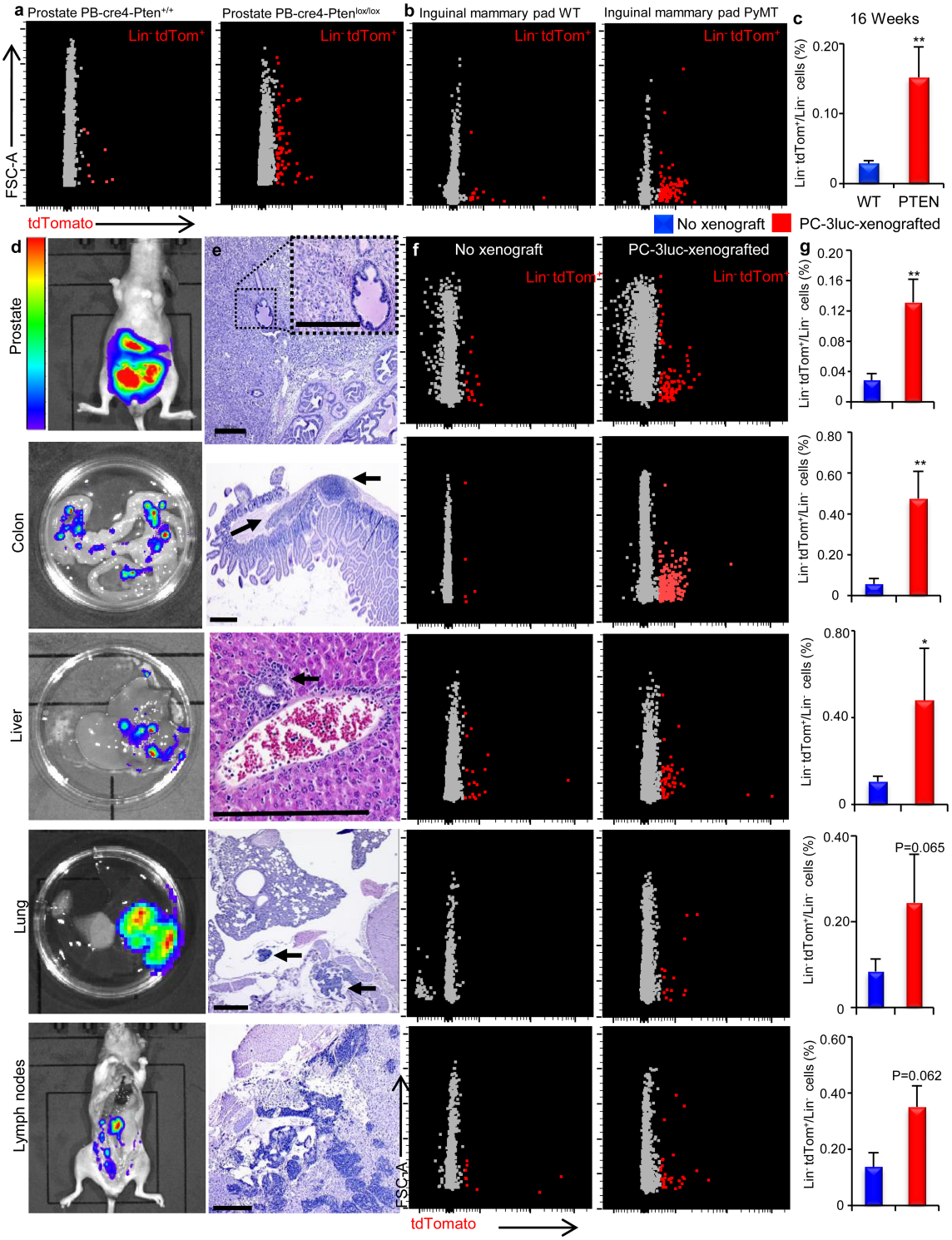

Extended Data Fig. 9 | Lin$^-$ tdTomato$^+$ cells can infiltrate Pten prostate tumours, PyMT breast tumours and metastases. a, **b**, After injection of a tdTomato-expressing lentiviral vector by stereotaxy into the SVZ at week 5 after birth, Lin$^-$tdTomato$^+$ cells are found at week 16 after birth in Pten prostate tumour tissues (**a**) or PyMT breast tumour tissues (**b**), by contrast to wild-type prostate or mammary pad tissues. **c**, Frequencies of Lin$^-$tdTomato$^+$ cells in Pten mice ($n = 5$) or wild-type littermates ($n = 8$). Data are mean + s.e.m. Student's *t*-test (one-sided, no adjustment). $^{**}P < 0.01$. Lin$^-$tdTomato$^+$ cells are also found in metastases. **d**, **e**, Luciferase-expressing human PC3 cancer cells orthotopically xenografted in the mouse prostate disseminate to colon, liver, lung and lymph nodes between 12 to 14 weeks after graft (**d**) and metastatic tissues were carefully dissected before be stained with a combination of haematoxylin and eosin (**e**). Scale bar, 300 μm. **f**, Neural progenitors transduced by a tdTomato-expressing lentiviral vector administered by stereotaxy into the SVZ, travel to PC3 xenografts and developing metastases in colon, liver, lung and lymph nodes at weeks 12–14 after graft. **g**, Frequencies of Lin$^-$tdTomato$^+$ cells in tumour tissues, listed above, by comparison to healthy tissues. Data are mean + s.e.m. Student's *t*-test (one-sided, no adjustment). $^*P < 0.05$, $^{**}P < 0.01$. Sample sizes per group are listed in Source Data. tdTom$^+$, tdTomato$^+$.

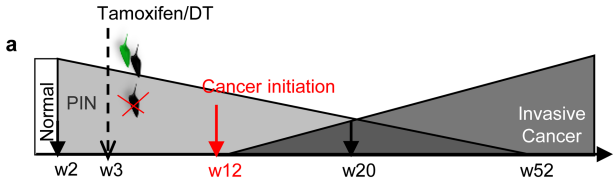

b

#	Tamoxifen/DT injections	Sacrifice
Protocol 1	w3 (IP)	w20
Protocol 2	w4 + w8 (IP)	w20
Protocol 3	w12 + w16 (IP)	w20
Protocol 4	w4(stereotaxic injection of DT into SVZ)	w20

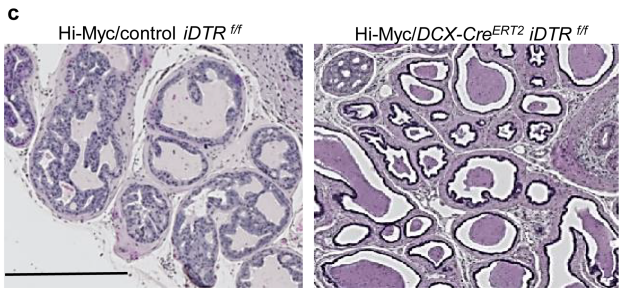

Extended Data Fig. 10 | Genetic depletion of DCX$^+$ cells. a, **b**, Timeline for MYC-induced tumour development, injections of tamoxifen and diphtheria toxin treatment 48 h after the last injection of tamoxifen (**a**) and experimental protocols (**b**). **c**, Representative H & E-stained sections of prostates of 20-week-old Hi-MYC mice.

nature research

Corresponding author(s): DBPR 2018-02-02263

Life Sciences Reporting Summary

Nature Research wishes to improve the reproducibility of the work that we publish. This form is intended for publication with all accepted life science papers and provides structure for consistency and transparency in reporting. Every life science submission will use this form; some list items might not apply to an individual manuscript, but all fields must be completed for clarity.

For further information on the points included in this form, see Reporting Life Sciences Research. For further information on Nature Research policies, including our data availability policy, see Authors & Referees and the Editorial Policy Checklist.

Please do not complete any field with "not applicable" or n/a. Refer to the help text for what text to use if an item is not relevant to your study.
For final submission: please carefully check your responses for accuracy; you will not be able to make changes later.

Experimental design

1. Sample size

   Describe how sample size was determined.

   Sample size was determined using G*Power software.

2. Data exclusions

   Describe any data exclusions.

   No data excluded

3. Replication

   Describe the measures taken to verify the reproducibility of the experimental findings.

   We have identified and characterized Doublecortin-expressing (DCX+) neural cells in the tumour microenvironment of 3 different models :
   -human cancer specimens.
   -orthotopic xenogeneic (luciferase-expressing PC-3 cancer cells) mouse cancer model.
   -transgenic (Hi-Myc, Pten, PyMT) mouse cancer models.

   To track and isolate DCX+ cells, we generated triple-transgenic cancer mice (DCX-CreERT2/ loxp-EYFP/Hi-Myc mice, called DCX-EYFP/Hi-Myc) and used flow cytometry and confocal image analyses as well as quantitative RT-PCR to characterize DCX+ cells in a reproducible manner.

   We have designed gain-and-loss of function studies using genetic (DCX-CreERT2/loxp-HBEGF/ Hi-Myc or nu/nu mice) and chemical (Tamoxifen/ Diphteria toxin) approaches combined with surgical transplantation of DCX+ cells.

   We have performed tdTomato lentiviral vector injections by stereotaxy in the SVZ/or DG of the 4 different mouse cancer models described above.

4. Randomization

   Describe how samples/organisms/participants were allocated into experimental groups.

   The effect of covariates on statistical comparisons was verified using regression analyses, as indicated on the method section.

5. Blinding

   Describe whether the investigators were blinded to group allocation during data collection and/or analysis.

   Human data collection:
   Quantification of DCX+ cells was conducted blind, without knowledge of clinical data, in prostate tumour or hyperplastic areas and in remaining normal prostate tissues surrounding cancer areas.

   Mouse data collection:
   Flow cytometry and bioluminescence data collection, and PIN quantifications were done blind.

Note: all in vivo studies must report how sample size was determined and whether blinding and randomization were used.

6. Statistical parameters

For all figures and tables that use statistical methods, confirm that the following items are present in relevant figure legends (or in the Methods section if additional space is needed).

n/a	Confirmed
☐	☒ The exact sample size (*n*) for each experimental group/condition, given as a discrete number and unit of measurement (animals, litters, cultures, etc.)
☐	☒ A description of how samples were collected, noting whether measurements were taken from distinct samples or whether the same sample was measured repeatedly
☐	☒ A statement indicating how many times each experiment was replicated
☐	☒ The statistical test(s) used and whether they are one- or two-sided *Only common tests should be described solely by name; describe more complex techniques in the Methods section.*
☒	☐ A description of any assumptions or corrections, such as an adjustment for multiple comparisons
☐	☒ Test values indicating whether an effect is present *Provide confidence intervals or give results of significance tests (e.g. P values) as exact values whenever appropriate and with effect sizes noted.*
☐	☒ A clear description of statistics including central tendency (e.g. median, mean) and variation (e.g. standard deviation, interquartile range)
☐	☒ Clearly defined error bars in all relevant figure captions (with explicit mention of central tendency and variation)

See the web collection on statistics for biologists for further resources and guidance.

Software

Policy information about availability of computer code

7. Software

Describe the software used to analyze the data in this study.

Live imaging software, version4.4 (Perkin Elmer, Waltham, MA) for bioluminescence analysis.
Flow Jo software (Tree Star, Ashland, OR).
Microsoft Excel 2011 (Microsoft, Redmond, WA).
GraphPad Prism7 software (GraphPad software, San Diego, CA).
LAS X 2.0.1.14392 software (Leica, Wetzlar, Germany).
Volocity 6.3.1 software (Perkin Elmer, Waltham, MA).
Zen microscope software (Zeiss MicroImaging, Thornwood, NY).
R software (https://www.r-project.org/, R Development Core Team, R Foundation for Statistical Computing, Vienna, Austria, version 3.3)

For manuscripts utilizing custom algorithms or software that are central to the paper but not yet described in the published literature, software must be made available to editors and reviewers upon request. We strongly encourage code deposition in a community repository (e.g. GitHub). *Nature Methods* guidance for providing algorithms and software for publication provides further information on this topic.

Materials and reagents

Policy information about availability of materials

8. Materials availability

Indicate whether there are restrictions on availability of unique materials or if these materials are only available for distribution by a third party.

No unique materials were used

9. Antibodies

Describe the antibodies used and how they were validated for use in the system under study (i.e. assay and species).

Flow cytometry
CD45 (clone 30F11), (Miltenyi biotec, Bergisch Gladbach, Germany).
TER119 (clone Ter-119), (Miltenyi biotec, Bergisch Gladbach, Germany).
CD31 (clone 390), (Miltenyi biotec, Bergisch Gladbach, Germany).
CD326 (clone caa7-9G8), (Miltenyi biotec, Bergisch Gladbach, Germany).
CD49f (clone REA518), (Miltenyi biotec, Bergisch Gladbach, Germany).
Sca-1 (clone REA422), (Miltenyi biotec, Bergisch Gladbach, Germany).
PSA-NCAM (clone 2-2B), (Miltenyi biotec, Bergisch Gladbach, Germany).
CD24 (clone M1/69), (Miltenyi biotec, Bergisch Gladbach, Germany).
Biotinylated EGF complexed with BV785-streptavidin (Invitrogen by Thermo Fischer Scientific).

Immunofluoresecnce
DCX (clone 2G5, lot VP1309040), (Millipore, Billerica, MA).
PSA-NCAM (clone 2-2B, cat: ABC-AbC0019), (ABC scientific, Los Angeles, CA).
βIII-tubulin (polyclonal,cat: PRB-435P, lot D13GF02055), (Covance, Princeton, NJ).
α-Internexin (polyclonal, AB5354, Lot 2208747) (Millipore, Billerica, MA).
EYFP (IgY fraction, cat: GFP-1020, Lot GFP697986) (Aves labs, Tigard, OR).
NF-H (Polyclonal, Cat : AB5539, Lot: 2219329) (Millipore, Billerica, MA).
Pan-cytokeratine (Monoclonal C-11, PCK-26, CY-90, KS-1A3, M20, A53-B/A2, Cat: C2562, Lot 033M4760V)(Sigma-Aldrich).
MAP-2 (Polyclona, Cat: AB5622) (Millipore, Billerica, MA).
CD31 (clone MEC13.3) (BioLegend, San Diego, CA)
Albumin (Polyclonal, Cat: GTX102419) (Genetex, Irvine, CA)
Alexafluor 647-, 568-, 488-conjugated goat antibodies to mouse, rabbit or chicken IgG respectively (Life technologies, Carlsbad, CA).
Primary antibodies were validated on mouse and human tissues.

10. Eukaryotic cell lines

a. State the source of each eukaryotic cell line used.

PC-3 cells (Human prostate adenocarcinoma) stably transfected with the luciferase 2 gene under the control of human ubiquitin C promoter have been provided by Perkin Elmer, Waltham, MA.

b. Describe the method of cell line authentication used.

The authentification of PC-3 cells was made by Perkin Elmer (Source of parental line ATCC CRL-1435TM)

c. Report whether the cell lines were tested for mycoplasma contamination.

All cell lines provided by Perkin Elmer (Caliper life sciences/Perkin Elmer) are confirmed to be pathogen free by the IMPACT profile I (PCR) at the university of Missouri research animal diagnostic and investigative laboratory.

d. If any of the cell lines used are listed in the database of commonly misidentified cell lines maintained by ICLAC, provide a scientific rationale for their use.

No commonly misidentified cell lines were used.

Animals and human research participants

Policy information about studies involving animals; when reporting animal research, follow the ARRIVE guidelines

11. Description of research animals

Provide all relevant details on animals and/or animal-derived materials used in the study.

Balb/c nu/nu (B6.Cg-Foxn1nu) and cMyc mice (FVB-Tg(ARR2/Pbsn-MYC)7Key21, called Hi-Myc hereafter) were obtained from Charles River laboratories and the National Cancer Institute, respectively.
Hi-Myc mice were intercrossed with C57BL/6-Gt(ROSA)26Sortm1(EYFP)Cos or C57BL/6-Gt(ROSA)26Sortm1(HBEGF)Awai/J mice which were previously crossed with Tg(DCX-cre/ERT2)1Mul mice to generate CreERT2-inducible expression of the enhanced yellow fluorescent protein (EYFP) or simian Diphtheria Toxin Receptor (DTR; from simian Hbegf) under the control of a doublecortin (DCX) promoter (all obtained from the Jackson laboratory). The resulting offsprings DCX-CreERT2/loxp-EYFP/Hi-Myc or DCX-CreERT2/loxp-HBEGF/Hi-Myc express EYFP or DTR, respectively, in DCX-expressing cells after administration of tamoxifen to the animals. Cells expressing DTR can be ablated following diphtheria toxin administration. Respective controls were also generated by intercrossing the three strains. Immunodeficient B6.Cg-Foxn1nu+/- heterozygous nude mice were also intercrossed with Tg(DCX-cre/ERT2)1Mul bred with Gt(ROSA)26Sortm1(HBEGF)Awai/J to deplete cells that express DCX in nu/nu mice.

Males (Hi-Myc or Pten lines) were used for all the experiments described in the manuscript (between week3 to week24 after birth).
Females (PyMT line) were used for experiments described in ED figure 10.
Males and females were used as breeders (between week6 and week16 after birth).

Policy information about studies involving human research participants

12. Description of human research participants

Describe the covariate-relevant population characteristics of the human research participants.

All patient and tumour characteristics were provided in Table 1 (age, gender, PSA levels, date of surgery, Gleason score, pathological stage, number of invaded zones, recurrence).
All patient had histologically confirmed and clinically localized prostate cancer or benign hyperplasia, and did not received prior treatment at the institution.